DOE/ET-53088-86 IFSR #86

THREE DIMENSIONAL STRUCTURE OF ICRF WAVES IN TOKAMAK PLASMAS

Kimitaka Itoh, Sanae-Inoue Itoh
Institute for Fusion Studies
The University of Texas at Austin
Austin, TX 78712

and

Atsushi Fukuyama
School of Engineering
Okayama University
Okayama 700, JAPAN

March 1983

Three Dimensional Structure of ICRF Waves in Tokamak Plasmas

Kimitaka Itoh*, Sanae-Inoue Itoh‡
Institute for Fusion Studies
The University of Texas at Austin
Austin, TX 78712

and

Atsushi Fukuyama
School of Engineering
Okayama University
Okayama 700, Japan

Permanent Address:

* Japan Atomic Energy Research Institute, Tokai, Ibaraki, 319-11, Japan

‡ Institute for Fusion Theory, Hiroshima University, Hiroshima, 730, JAPAN.

ABSTRACT

The three-dimensional structure of the ICRF (Ion Cyclotron Range of Frequencies) waves in a tokamak plasma is studied. The toroidal field gradient, radial density inhomogeneity and the poloidal-toroidal localizations of the antenna current are incorporated. The ICRF wave propagation and absorption in the two-ion species plasma (majority deuterion and minority hydrogen) are obtained by numerically solving the propagation equations in collisional cold plasmas. Two cases of the heating mechanisms, the ion-ion hybrid resonance and the cavity resonance (i.e., the forced excitation of damped eigenmode) are found in a three-dimensional configuration. Owing to the lack of homogeneity in the up-down direction, the global wave form, energy deposition profile and total energy absorption are affected, and considerable differences from the two-dimensional calculations are found. In the case of the ion-ion hybrid resonance, the energy deposition profile is localized near the hybrid resonance surface; the energy absorption integrated over the plasma column is independent of the damping rate. On the contrary, the cavity resonance realizes a strong heating over the whole plasma column by a coherent wave, which satisfies the cavity resonance condition. This heating occurs in the absence of the cyclotron and the hybrid resonances. When we calculate the loading impedance by the poloidal current antenna with Faraday shield, we find that the cavity resonance can contribute to the wave absorption as much as (or more than) the ion-ion hybrid resonance for wide range of plasma parameters.

1. Introduction

The problems of ICRF (ion cyclotron range of frequency) waves have attracted attentions. Recent experimental results have shown the effectiveness of ICRF waves in the high-power heatings.[1] The ICRF waves also have the potentialities in applications to improve confinement, f.g., the current-drive, radial cross-field flux control,[2] impurity flow control,[3] and end pluggings.[4] In spite of such high potentialities, the analyses on ICRF waves seems to be unsatisfactory. Analyses based on the local dispersion relation have shown[5] (1) the possible damping mechanisms of the waves, i.e., the Landau and cyclotron resonances, (2) ion-ion hybrid resonance and (3) the mode conversion characters. The ray tracing method has been applied to study the energy deposition in tokamak configurations.[6] However the global wave propagation form and deposition profile cannot be obtained, since the wave length can be comparable to the scale lengths of plasma inhomogeneities.

To study the global wave form and the coherent nature of the waves, the wave propagation equations have been solved as stationary boundary value problems. The collisional MHD analyses can resolve the total absorption power for given antenna condition. In the two-dimensional model, where inhomogeneity in the equitorial surface is taken and the variations in the poloidal direction are neglected, MHD model was solved[7] to give the antenna loading resistance and has shown the importance of the global wave form. We have recently derived the kinetic equations for the study of propagation and absorption of ICRF waves,[8] and solved in the two-dimensional model.[9] The consistent profile of energy deposition for each plasma species as well as the

loading resistance has been obtained for given launching conditions. It has been shown that the cavity resonance[7,10] exists and allows efficient energy flow from the antenna to the plasma;[9] the cavity resonance has also been found in experiments.[11,12] Theoretically there still has been a question whether this coherent nature of waves obtained in the 2-D calculation is valid in the realistic three-D plasma geometry. The plasma has radial inhomogeneity, such as the density, while the magnetic field strength changes in the major radius direction. In addition to it the antenna has the finite extent in the toroidal and poloidal directions. Three-dimensional analyses are desired 1) to resolve the question above, 2) to obtain the total loading and 3) to compare the heating efficiencies between the ion-ion hybrid resonance and the cavity resonance.

In this article we study the three-dimensional structure of the ICRF waves in a tokamak plasma, by numerically solving the collisional MHD equations. The toroidal field gradient, radial density inhomogeneity and the localization of the antenna current in the poloidal-toroidal directions are incorporated. The collisional damping is introduced to get rid of the divergence of the conductivity tensor at cyclotron and hybrid as well as cavity resonances. The ICRF wave propagation and absorption in the two-ion species plasma (majority deuterium and minority hydrogen) are obtained. The two-ion hybrid resonance and the cavity resonance are demonstrated in the three-dimensional configurations. In the ion-ion hybrid resonance case, the energy absorption $\dot{W}(\vec{r})$ is localized near the hybrid resonance surface. The energy absorption over the plasma column, $\int \dot{W}\, d^3\vec{r}$, is independent of the choice of damping rate in the small collisionality

limit. On the contrary, the cavity resonance realizes a strong heating over the whole plasma column. The total absorption over the radiated spectrum shows that the cavity resonance can contribute considerably to the wave absorption for wide range of plasma parameters.

2. Model and Basic Equations

We take a toroidal plasma with the minor radius a and the major radius R. The plasma is surrounded by a perfect conducting shell of the radius b, the geometric center of which is assumed to coincide with the magnetic axis of the plasma. The toroidal coordinates (r,θ,ϕ) are used, where r is the minor radius, θ and ϕ are the poloidal and toroidal angles respectively.

In this article we study the ICRF waves excited by the poloidal current antenna. The antenna is simulated by the poloidal current sheet on the surface r=d which is given as

$$\tilde{J}_A(\vec{r},t) = \sum_{\ell,M} \tilde{J}_{M,\ell}\ \delta(r-d)\exp(iM\theta - i\ell\phi - i\omega t)\ . \tag{1}$$

where $\delta(r-d)$ is the delta function and tilde denotes oscillating components. Since the plasma is assumed to have the axial symmetry, each ℓ component can be treated separately. The Faraday shield is simulated by the condition $\tilde{E}_\phi = 0$ at the antenna where r=d.

The equations which dictate the electromagnetic field based on the MHD approximations in the plasma are given, in the (x,y,z) coordinates ($x=r\cos\theta$, $y=r\sin\theta$, $z=R\psi$), as

$$\nabla \times \nabla \times E - \frac{\omega^2}{c^2} \begin{bmatrix} S & -iD & 0 \\ iD & S & 0 \\ 0 & 0 & P \end{bmatrix} \vec{E} = 0 \tag{2}$$

where

$$S = 1 - \sum_{\sigma} \frac{\omega_{p\sigma}^2}{\omega^2 - \Omega_\sigma^2} \quad , \tag{3}$$

$$D = - \sum_{\sigma} \frac{\omega_{p\sigma}^2 \Omega_\sigma}{\omega(\omega^2 - \Omega_\sigma^2)} \quad , \tag{4}$$

$$P = 1 - \sum_{\sigma} \frac{\omega_{p\sigma}^2}{\omega^2} \quad , \tag{5}$$

$\omega_{p\sigma}^2 = n_\sigma q_\sigma^2 / m_\sigma \varepsilon_0$, $\Omega_\sigma = q_\sigma B_0 / m_\sigma^*$ and $m_\sigma^* = (1 + i\nu_\sigma/\omega) m_\sigma$. The suffix σ denotes the particle species, q_σ and m_σ particle charge and mass, n is the number density, and ν_σ is introduced as a model collision frequency, which eliminates the divergent behavior of S and D at $\omega = \Omega_\sigma$. In Eq. (2), the strong toroidal magnetic field is given as,

$$B_0 = \frac{B}{1 + \frac{r}{R}\cos\Theta} \quad , \tag{6}$$

and the rotational transform and the diamagnetic well by the plasma pressure are neglected. We are interested in the case of tokamak plasmas where $P >>> 1$ holds in Eq. (2), i.e., the parallel electron conductivity is large. The parallel electric field perturbation is small in comparison with the perpendicular electric field component, and the excitation of $\tilde{E}_\phi$ is also eliminated by the Faraday shield. We therefore neglect $\tilde{E}_\phi$ and solve the $\tilde{E}_r$ and $\tilde{E}_\Theta$ components. We have ($k_\parallel = \ell/R$)

$$\frac{1}{r^2}\frac{\partial^2}{\partial\Theta\partial r}\,rE_r - \frac{1}{r^2}\frac{\partial^2}{\partial\Theta^2}\,E_\Theta + \left(k_\parallel^2 - \frac{\omega^2}{c^2}\,S\right)E_r + \frac{i\omega^2}{c^2}\,D\,E_\Theta = 0 \tag{7}$$

$$-\frac{\partial}{\partial r}\frac{1}{r}\frac{\partial}{\partial r}\,rE_\Theta + \frac{\partial}{\partial r}\frac{1}{r}\frac{\partial}{\partial\Theta}\,E_r - \frac{i\omega^2}{c^2}\,D\,E_r + \left(k_\parallel^2 - \frac{\omega^2}{c^2}\,S\right)E_\Theta = 0 \tag{8}$$

In the vacuum region, we solve Eqs. (7) and (8) setting S=1 and D=0.

The boundary conditions we employ are

$$\begin{pmatrix} r\tilde{E}_r \\ r\tilde{E}_\Theta \end{pmatrix} \to 0 \qquad \text{as } r \to 0 \tag{9}$$

$$\begin{pmatrix} \tilde{E}_\Theta \\ \tilde{B}_r \end{pmatrix} \to 0 \qquad \text{as } r \to b \tag{10}$$

at the magnetic axis and on the shell, and

$$\tilde{B}_\phi(d+0) - \tilde{B}_\phi(d-0) = \mu_0\tilde{J} \tag{11}$$

at the antenna.

Before solving the full set of the wave propagation equations, let us consider the characteristic surfaces related to the ICRF propagation and absorption. If the local approximation is employed, i.e. $\nabla \to i\vec{k}$, Eq. (2) gives

$$k_\perp^2 = \frac{\left(\frac{\omega^2}{c^2} S - \frac{\omega^2}{c^2} D - k_\parallel^2\right)\left(\frac{\omega^2}{c^2} S + \frac{\omega^2}{c^2} D - k_\parallel^2\right)}{\frac{\omega^2}{c^2} S - k_\parallel^2} . \qquad (12)$$

The ion-ion hybrid resonance surface where $k_\perp^2$ becomes very large is given by

$$S = \frac{c^2}{\omega^2} k_\parallel^2 , \qquad (13)$$

and the cut-off surface where $k_\perp^2$ vanishes (in the limit $\nu \to 0$) is given by

$$S = \pm D + \frac{c^2}{\omega^2} k_\parallel^2 . \qquad (14)$$

The elements S and D depend on x through Ω_σ and on r through $n_\sigma(r)$ and the structure of these surfaces defined by (13) or (14) are to be described on two-dimensional poloidal cross-section in addition to the toroidal angle.

3. Analysis of the Wave Propagation and Absorption

The equations (7) and (8) are numerically solved with the boundary conditions (9)-(11). (The numerical procedure is briefly shown in the appendix.) To study the three-dimensional mode structure, we first consider the case of the M=0 symmetric antenna and compare with the results with 2-D analyses. Two basic mechanisms of the wave absorption are also found in 3-D case; the ion-ion hybrid resonance and the cavity resonance. Then we examine the high-field-side excitation and the low-field-side excitation.

3-1. M=0 Antenna

The case of M=0 antenna is studied by taking

$$\tilde{J}_A(\vec{r},t) = \sum_{k_\parallel} \tilde{J}(k_\parallel,\omega)\delta(r-d)\exp(ik_\parallel z - i\omega t) \ , \tag{15}$$

and each $k_\parallel$ component is treated separately. We study the two ion component plasma (minority hydrogen and majority deutrium) and take the parameters $b/a = 1.5$, $d/a = 1.1$, $a/R = 0.2$, $n_H/n_D = 0.1$, $\omega_{pD}^2(0)/\Omega_D^2(0) = 10^3$, $a^2\Omega_D^2(0)/c^2 = 5 \times 10^{-2}$ and $M_H/M_e = 1836$ as standard values. The density profile $n(r)/n(0)$ is given as

$$n(r)/n(0) = 1 - r^2/a^2 \ . \tag{16}$$

The local energy deposition $\dot{W}(r,\Theta) \equiv \langle \tilde{\vec{J}} \cdot \tilde{\vec{E}} \rangle$ (the bracket denotes an average over the wave period) is calculated by the relation

$$\dot{W}(r,\theta) = \frac{1}{\omega\mu_0 a^2}\frac{a^2\omega^2}{c^2}\{\mathrm{Im}S|\tilde{E}_\perp|^2 + 2\ \mathrm{Im}D\ \mathrm{Im}(E_r^* E_\theta)\} \tag{17}$$

where * shows the complex conjugate. The total absorption per unit length of the plasma column, P_{abs}, is given by

$$P_{abs}(k_\parallel,\omega) = \int_0^{2\pi} d\theta \int_0^a r dr\ \dot{W}(r,\theta)\ . \tag{18}$$

The loading resistance $\hat{R}$ is calculated as

$$\hat{R}(\omega) = \frac{2\pi R\int dk_\parallel P_{abs}(k_\parallel,\omega)}{I^2} \tag{19}$$

where I is the total current on the antenna. If one specifies the toroidal width of the antenna current, the spectrum $\tilde{J}(k_\parallel)$ is determined and $\hat{R}$ is calculated.

[A]. Ion-ion Hybrid Resonance

The Figure 1(a) and (b) shows the contour of $\dot{W}(r,\theta)$ on the cross-section of the plasma column for the parameters $\omega/\Omega_D(0) = 1.75$, $\nu/\omega = 10^{-2}$ and $k_\parallel a = 2$ (a) and 4(b). The dotted line shows the ion-ion hybrid resonance surface where $\mathrm{Re}\ S = c^2k_\parallel^2/\omega^2$ holds, on which $k_\perp$ becomes very large. It is clearly shown that the energy deposition is strongly localized near the ion-ion hybrid resonance surface with the HWHM (half-width at half-maximum) which is proportional to ν. The noticeable is, however, the structure of $\dot{W}$ on the resonance surface. The case (a) ($k_\parallel a$=2) shows the power deposition is peaked near $y \simeq 0$

and slowly decreases as $|y|$ increases. The electric field amplitude is not uniform when y changes. As $k_\parallel$ changes, the amplitude of $\tilde{E}$ at the point, where $y = 0$ and $\mathrm{Re}\ S = k_\parallel^2 c^2/\omega^2$ hold, becomes small, and the peak of $\dot{W}(r,\theta)$ moves towards the point of the large value of $|y|$. The energy deposition $\dot{W}(r,\theta)$ has another broad and low peak near the plasma axis. This is because we keep the collisional damping and n(r) becomes large near the plasma center. This contribution vanishes in the $\nu \to 0$ limit. It is noted that the up-down symmetry is violated. The symmetry holds in the transformation $y \to -y$ and $B \to -B$.

The major contribution to the energy absorption in this case is not the collisional dissipation, but the ion-ion hybrid resonance, as is shown in the ν/ω dependence of P_{abs}. The Figure 2 illustrates the ν/ω dependences of P_{abs} and the peak value of $\dot{W}$ for the fixed value of $\tilde{J}$. We choose $\omega/\Omega_D(0) = 1.75$ and $k_\parallel a = 1$, and P_{abs} and $\dot{W}_{max}$ are measured in arbitrary units. It is found that $\dot{W}_{max}$ is proportional to $(\nu/\omega)^{-1}$, while the half-width is proportional to ν/ω. Therefore the total absorption is almost independent of the dissipation rate ν/ω. These features are characteristic to the power absorption associated with the spatial resonance surface.[13]

Another feature of the ion-ion hybrid resonance lies in the broad $k_\parallel$ dependence of P_{abs}. This is because the excited wave energy is converted to the so-called "continuous spectrum" which is given by the condition $k_\parallel^2 c^2/\omega^2 - S = 0$ $(\nu \to 0)$. The slow dependence on $k_\parallel a$ is shown in Fig. 3. The bump in the higher $k_\parallel a$ tail is the contribution of the cavity resonance, which is studied in detail later. The absorption P_{abs} or the coupling becomes very small for the large value of $k_\parallel$. This is because the evanescent layer defined by

$$k_{\parallel}^2 \gtrsim \frac{\omega^2}{c^2}(S - D) \tag{20}$$

(or approximately $k_{\parallel}^2 \gtrsim \omega^2/v_A^2$, v_A: Alfvén velocity) near the plasma periphery becomes wide as $k_{\parallel}$ increases. The dotted line in Fig. 3 is for the case of much peaked density profile,

$$n(r)/n(0) = (1-r^2/a^2)^2$$

which has the wider evanescent layer; in this case the decrease of P_{abs} starts much lower values of $k_{\parallel}$. The arrows on the curves indicate the condition that the width of the evanescent layer (at $\Theta=-\pi$) becomes $a/2\pi$.

The toroidal wave form and absorption profile are reconstructed from the $k_{\parallel}$ dependence of $P_{abs}(k_{\parallel})$. When the toroidal extent of the antenna is denoted by L_t, the spectrum of $\tilde{J}(k_{\parallel})$ is typically given

$$J(k_{\parallel}) \sim \begin{cases} I/\pi R & |k_{\parallel}| \lesssim L_t^{-1} \\ 0 & |k_{\parallel}| \gtrsim L_t^{-1} \end{cases} . \tag{21}$$

The upper limit of the parallel wave number $k_{\parallel}$ of the accessible waves may be given by the $k_{\parallel c}$ which is defined by the condition that the radial thickness of the peripheral evanescent layer becomes $a/2\pi$, i.e.,

$$k_{\parallel c}^2 \sim \frac{\omega^2}{c^2}(S - D)\Big|_{r=a-a/2\pi} . \tag{22}$$

Among the components which are excited in the plasma, (i.e., $|k_\parallel| \lesssim L_t^{-1}$), the accessible components satisfying $|k_\parallel| \lesssim k_\parallel^c$ propagates inside of the plasma and has large amplitude near the ion-ion hybrid resonance. Fourier composing the excited components ($|k_\parallel| \lesssim L_t^{-1}$, $k_\parallel^c$) one finds that the rf wave amplitude is localized in toroidal direction. The maximum point is close in front of the antenna and the length of toroidal localization, ℓ_t, can be approximately evaluated as

$$\ell_t \simeq \max(k_{\parallel c}^{-1}, L_t) . \tag{23}$$

In the limit $L_t \to 0$, the wave is localized in toroidal direction with coherent length $\sim k_{\parallel c}^{-1}$.

[B]. Cavity Resonance

The study of the frequency dependence of P_{abs} reveals successive sharp peaks in the wider range of parameters. In the cases where P_{abs} shows peaks, the ion-ion hybrid resonance surface is not necessarily located in the plasma column. The Figure 4 shows the contour map of $P_{abs}(k_\parallel, \omega)$ on the $(k_\parallel, \omega)$ plane for fixed values of $\tilde{J}_\parallel$. The broad peak in the region $1.6 \lesssim \omega/\Omega_D(0) \lesssim 2.2$ is due to the ion-ion hybrid resonance. The successive prominent peaks are seen along the hyperbolic lines. These peaks appear due to the cavity resonance formations (or in other words, the peaks show the existence of weakly damped eigenmodes).

The nature of the cavity resonance is different from the ion-ion hybrid resonance. The energy is deposited over the whole plasma column with the fairly good symmetry in the poloidal direction. The energy absorption mechanism, in this case, is the collisional damping. The Figure 5 shows the typical deposition profile $\dot{W}(r,\theta)$ on the y=0 midplane. This resonance corresponds to the 5-th harmonic of the symmetric eigenmodes. When the forced oscillation is applied near the weakly damped eigenmode, the oscillation amplitude is proportional to ν^{-1} and hence the absorption power ($\sim \nu\tilde{E}^2$) is also proportional to ν^{-1}. The Figure 6 shows the ν/ω dependences of $|\tilde{E}|$, the peak value $\dot{W}$ and P_{abs}, and confirms the ν-dependences to be ν^{-1}. The $k_\parallel$ dependence of P_{abs} is shown in Figure 7 for $\omega/\Omega_{DO} = 2.5$ and ν/ω is chosen to be 0.015, 0.01 and 0.005. The Lorentz type peak,

$$P_{abs}(k_\parallel) \propto \frac{\Delta k_\parallel}{[k_\parallel - k_{\parallel r}(\omega)]^2 + \Delta k_\parallel^2} \tag{24}$$

where $\Delta k_\parallel$ is proportional to ν/ω, is clearly shown. Since the actual antenna has the small and finite extent in the toroidal direction, L_t, the broad spectrum of the rf wave, $|k_\parallel| \lesssim L_t^{-1}$, is emitted. When the toroidal periodicity length $2\pi R$ is larger than $(\Delta k_\parallel)^{-1}$, then the total absorption over the plasma,

$$P_{tot} \equiv \sum_{\ell} 2\pi R P_{abs}(k_\parallel, \omega)$$

($k_\parallel = \ell/R$), is approximated by the integral $\int d(Rk_\parallel) 2\pi R P_{abs}$. If the launched spectrum is wide enough,

$$|k_{\parallel r}(\omega)| < L_t^{-1} , \tag{25}$$

then the integralation is performed and P_{tot} is independent of ν/ω.

The existence of the cavity resonance affects the loading impedance. When the broad spectrum of the rf wave is excited, the total absorption P_{tot} has weak dependence of ω provided that the resonance $k_{\parallel r}(\omega)$ is much smaller than the "cut-off" $k_{\parallel c}$ defined by Eq. (22). If the plasma density is high then many resonances appear for given ω and the differences of $k_{\parallel r}$ between two successive resonance becomes smaller than $k_{\parallel c}$. Then the contribution of cavity resonances always contributes to P_{tot} and the total absorption shows a weak dependence on ω. The Figure 8 shows $\hat{R}$ as a function of ω. For this case, the differences of two successive $k_{\parallel r}(\omega)$ is of the order of $k_{\parallel c}$ and the peak of $\hat{R}$ becomes much broader than Figure 4. It is noted that the width of the peaks of $\hat{R}$ reflects the cut-off layer near the surface, not the width by ν/ω. The peak of $\hat{R}$ is about twice of the bottom of $\hat{R}$, which is almost independent of ν. The peak of $P_{abs}(k_\parallel,\omega)$ is proportional to $1/\nu$, while the integral $\int P_{abs}\, dk_\parallel$ is almost independent of ν. In calculating the loading resistance $\hat{R}$, we have chosen the antenna width such that $L_t \sim k_{\parallel c}^{-1}$.

The resonance condition is numerically found to be in the form, $k_\parallel = k_{\parallel r}(\omega)$, where

$$\omega^2 = \overline{V}_{An}^2 \left(K_n^2 + k_\parallel^2 \right) \tag{26}$$

$\overline{V}_{An}$ is the typical value of the Alfvén velocity, and K_n is the perpendicular wave number of the n-th harmonics. Let us analyze this

condition. When one considers the case where the hybrid resonance condition is not satisfied in the plasma column, the x-dependence of the conductivity tensor which is originated from the x-dependence of Ω becomes weak and unimportant. The poloidal-symmetric, M=0 resonance condition is dictated by the equation ($g=rE_\theta$)

$$\frac{c^2}{\omega^2} r \frac{d}{dr} \frac{1}{r} \frac{d}{dr} g + \frac{(S-D-k_\parallel^2 c^2/\omega^2)(S+D-k_\parallel^2 c^2/\omega^2)}{S-k_\parallel^2 c^2/\omega^2} g = 0 \qquad (27)$$

with the boundary condition g=0 at r=0 and r=b. This equation determines $\bar{V}_{An}^2$ and K_n^2. The critical condition for the appearance of n-th resonance, which has n-radial nodes, is calculated by letting $k_\parallel=0$ as

$$\frac{c^2}{\omega^2} r \frac{d}{dr} \frac{1}{r} \frac{d}{dr} g + \frac{S^2-D^2}{S} g = 0 \qquad (28)$$

If the cyclotron resonance of minority is unimportant, then the effective "potential" $(S^2-D^2)/S \sim \omega_{pD}^2/\omega^2$ is proportional to the density. The critical density for the n-th eigenmode is calculated from Eq. (28). Taking the simplified limit $\omega \gg \Omega_D$ and $\eta \ll 1$, and letting $k_\parallel$ be zero, one has

$$\omega^2 = \frac{\lambda_n}{a^2} v_A^2(0) \qquad (29)$$

where λ_n is the n-th eigenvalue of the equation

$$\left[u \frac{d}{du} \frac{1}{u} \frac{d}{du} + \lambda_n(1-u^2)\right] g_n = 0 \ . \tag{30}$$

Taking $k_\parallel^2$ into account perturbatively we have the cavity resonance condition between ω and $k_{\parallel r}$ as

$$\omega^2 \simeq V^2_A(0)\left[\frac{\lambda_n}{a^2} + \frac{\int du |g_n|^2/u}{\int du |g_n|^2(1/u-u)} k^2_{\parallel r}\right] \ . \tag{31}$$

This condition shows hyperbolic relation between ω and $k_{\parallel r}$; this result agrees with the numerical calculations.

The toroidal mode structure in the presence of the cavity resonance is quite different from the case of the hybrid resonance. Let us consider the case, for example, where one resonance is accessible (i.e., only one $k_{\parallel r}$ satisfies $k_{\parallel r} < k_{\parallel c}$ for given ω), and wide spectrum is radiated from antenna (i.e., $1/L_t \gtrsim k_{\parallel c}$). Then among the waves which are excited in the plasma, only cavity mode has large amplitude ($\tilde{E} \propto (\nu/\omega)^{-1}$) with the bandwidth $\Delta k_\parallel$. Therefore the Fourier composed wave is dominated by the cavity mode and the coherence length in the toroidal direction ℓ_t is estimated to be

$$\ell_t \sim \Delta k_\parallel^{-1} \ . \tag{32}$$

Noting the relation $\Delta\omega/\omega \sim \nu/\omega$ and $\Delta\omega/\omega \sim \Delta k_\parallel k_\parallel/(k_\parallel^2+K_n^2)$, ℓ_t can easily reach the toroidal length $2\pi R$: as a result of the fact, a coherent single mode is observed in a toroidal plasma even if the wave is excited by a toroidally-localized antenna.[14]

3-2. High-Field Side and Low-Field-Side Excitations

We first compare the cases of the high-field-side (HFS) excitation and low-field-side (LFS) excitation by choosing the Θ-dependent current as

$$\tilde{J_A}(\Theta) \sim \begin{cases} 1 + \frac{3}{2}\cos\Theta + \frac{3}{5}\cos 2\Theta + \frac{1}{10}\cos 3\Theta & \text{(LFS)} \quad (33\text{-}1) \\ 1 - \frac{3}{2}\cos\Theta + \frac{3}{5}\cos 2\Theta - \frac{1}{10}\cos 3\Theta & \text{(HFS)} \; . \quad (33\text{-}2) \end{cases}$$

The width at the half maximum of J_A is approximately $3\pi d/10$. The Figure 9 shows the power deposition profile on the midplane (y=0) for the parameters $\omega/\Omega_D(0) = 2$ and $k_\parallel a = 1.5$ (LFS), 2.5 (HFS). In the low-field-side excitation, the wave becomes evanescent at the cut-off surface

$$D \simeq S$$

which intercepts the resonance surface from the antenna. Almost all energy is deposited through the collisional damping over the whole plasma column. On the contrary, in the high-field-side excitation case, the wave energy is absorbed by plasmas near the ion-ion hybrid resonance surface through the hybrid resonance.

This result illustrates a one basic feature of the LFS and HFS excitations. The other issue is to know the effect of the "finite length" of the antenna. We therefore take the current of the antenna as

$$\tilde{J}_A(\Theta) \sim \begin{cases} J_0 \sum_{n=-\infty}^{\infty} \exp\left[-\left(\frac{\Theta - 2n\pi}{\pi\Delta}\right)^2\right] & \text{(LFS)} \quad (34\text{-}1) \\ J_0 \sum_{n=-\infty}^{\infty} \exp\left[-\left(\frac{\Theta - 2n\pi + \pi}{\pi\Delta}\right)^2\right] & \text{(HFS)} \quad (34\text{-}2) \end{cases}$$

to study the effect of the finite poloidal length of the antenna. The normalization coefficient J_0 is chosen such that $J_A(0) = 1$ (LFS) or $J_A(\pi) = 1$ (HFS) is satisfied. The parameter Δ denotes the localization in the poloidal angle. When Δ is small, the antenna is localized near $x \simeq \pm d$. As Δ increases the length increases and the result approaches to the M=0 antenna.

We first study the high-field-side excitations. In this case the wave is accessible to the ion-ion hybrid resonance region provided that the evanescent layer at x=-a is not thick, i.e., $k_\parallel < k_{\parallel c}$. The Figure 10 shows Δ dependence of P_{abs} for the parameters $k_\parallel a = 1.5$, $\nu/\omega = 10^{-2}$ and $\omega/\Omega_D = 1.75$ and 2.0. As is discussed in Section 3-1, the absorption P_{abs} is nearly independent on the choice of ν/ω. From the figure one sees

$$P_{abs} \propto \Delta , \tag{35}$$

and the power absorption per unit length of the antenna, $P_{abs}/a\Delta$ can be defined. This value is to be compared to the two-dimensional MHD calculation where the nonuniformity in y-direction is neglected. The two-dimensional calculation gives a good quantitative argument.

We next study the low-field-side excitations. The ion-ion hybrid resonance layer is not accessible due to the cut-off layer, according to the local theory. Therefore the wave can propagate to the resonance layer either by the tunneling or by the diffraction which is expected when the poloidal length of the antenna is large enough. By studying the ν/ω dependence of P_{abs}, we can tell whether the propagation of the wave to the resonance layer is prohibited or not. If prohibited, then

the absorption P_{abs} is proportional to ν/ω. However, when the wave propagates to the resonance layer then P_{abs} shows much slower dependence on ν/ω. The transition between these two typical dependences on ν/ω is expected to occur at a certain value of Δ above which the wave is accessible. We study the ν/ω dependence of P_{abs}, which is shown in Fig. 11 for the parameters $k_{\parallel} a = 1.5$. $\omega/\Omega_D(0)$ is chosen to be 1.75 and 2.5; in the former case there exists a ion-ion hybrid resonance surface in the plasma while in the latter case not. When Δ is small (Δ=0.2), P_{abs} is proportional to ν/ω, independent of the existence of the hybrid resonance surface. The evanscent layer is thick and the tunneling is not effective for the parameter ($\nu/\omega \lesssim 10^{-2}$). On the contrary, if Δ becomes large (Δ=0.5), the poloidal-radial structure becomes important and the wave can penetrate to the high-field side by the diffraction and refraction. The ν-dependence is much weaker and P_{abs} may remain finite in the $\nu \to 0$ limit.

The typical feature of the $k_{\parallel}$ dependence is the same as the M=0 antenna case. Also the broad $k_{\parallel}$ dependence of P_{abs} is found for the ion-ion hybrid resonance heating case (HFS case). Cavity resonances which is found in Section 3-1 is also obtained. In LFS (or HFS) excitation case new resonances appear. The M=0 antenna excites the "M=0" eigenmode (no poloidal node), but the LFS or HFS case can excite the eigenmode with poloidal node. The absorption profile $\dot{W}(r,\Theta)$ on the midplane (y=0) shows that the number of the local peaks is an odd number.

The Figure 12 shows the Poynting vector on the radial-poloidal plane for the low-field excitation. Radial-poloidal structure is clearly shown. It should be noted that the Poynting vector near the surface is not perpendicular nor parallel to the surface; the direction is determined self-consistently by the global wave form, and the arbitrary choice such as the assumptions on the initial condition of the ray trajectory is not allowed.

4. Summary and Discussions

In summary, we have investigated the three-dimensional structure of ICRF waves in toroidal plasmas developing the numerical method based on the MHD analyses. The two ion species plasma is investigated.

Due to the toroidal field inhomogeneity, the conductivity tensor has strong x-dependence especially near the ion-ion hybrid resonance and cut-off surfaces, in addition to the radial density inhomogeneity. These two inhomogeneities are intrinsic to the plasma response to the ICRF waves, so that the three-dimensional analysis is inevitable to know the wave form or the power deposition profile. In addition to it, the boundary condition plays essential roles in determining the wave forms in the plasma as well as the loading impedance of the plasma. We show the wave form in a realistic geometry, including such as the plasma-vacuum interface, antenna and conducting walls.

The two ways of the energy absorption are clarified. One is the usual ion-ion hybrid resonance, and the other is due to the cavity resonance. The former mechanism yields a broad $k_{\parallel}$ coupling to the antenna, and the energy is absorbed by the continuous spectrum near the ion-ion hybrid resonance surface. The latter mechanism is essentially the forced oscillation in the vicinity of the weakly damped eigenmode. Almost all energy is converted to the eigenmode, and the energy is deposited over the whole plasma column. If the damping is weak, the peak of the loading resistance $P_{abs}(k_{\parallel},\omega)$ becomes very sharp. However, when the antenna radiates a wide $k_{\parallel}$ spectrum due to the finite toroidal width, the total absorption is independent of the damping rate and is proportional to the number of eigenmodes which satisfies the accessibility condition

$$|k_{\parallel r}| \lesssim k_{\parallel c}(\omega) .$$

Parameter dependence of the loading resistance changes quite a lot depending on how many cavity resonances exist in the region $|k_\parallel| \lesssim k_{\parallel c}$. Experimentally sharp peaks of the loading resistance have been observed.

From the $k_\parallel$ dependence of P_{abs} we obtain a condition for the toroidal width of the antenna. Since the Fourier components which satisfies the condition $|k_\parallel \gtrsim k_{\parallel c}$ are not absorbed but repelled by the cut-off layer at the plasma surface, these components increase the loading reactance but does not contribute to the resistance. In order to reduce the reactance, such high $k_\parallel$ components must not be radiated from the antenna; the toroidal width of the antenna, L_t, must be comparable or greater than $k_{\parallel c}^{-1}$.

The radial-poloidal structure is obtained and the effect of the finite antenna length in the poloidal direction is found important. In the high-field-side excitations, the deviation from the two-dimensional analysis is, at least qualitatively, fairly small. However, in the low-field-side excitations, the refractions and diffractions become important and the two-dimensional analysis is not always satisfactory. In this article, we study the case where the antenna has up-down symmetry. The actual experiment sometimes has the upper-quarter antenna. Our method can be directly applied to these kind of cases; also can be applicable to the noncircular cross-section plasma or shell and the deformed antenna. The excitation by the wave guide is also analyzed by a straight-forward extension.

The parameter ν is introduced to simulate the collisional dissipation which also can get rid of the numerical divergence at the resonances. In the ion-ion hybrid resonances, P_{abs} is independent of ν/ω if ν/ω is chosen small enough, showing that the calculated wave form correctly keeps the character of the "continuous spectrum". This is the case where the loss at the wall is neglected. The MHD analysis is not sufficient to describe the thermalization process of the absorbed energy or cannot include the mode conversion to the ion-Bernstein mode. The actual energy deposition profile can be calculated if the present analysis is extended to the kinetic theory.

The cavity resonance indicates the weakly damped eigenmode. The damping rate of corresponding eigenmode, γ, is estimated by the half-width at half maximum of the peaks of $P_{abs}(k_{\parallel},\omega),\Delta\omega$. From Fig. 4 we see that $\Delta\omega/\omega \sim \gamma/\omega$ and the damping rate is very weak. Therefore the eigenmode can easily be destabilized by high energy beams or other rf waves. The damping rate and the excitation rate by the extra free energy source are to be determined by the kinetic treatment of the plasma conductivity. The threshold for the onset of the instability of the eigenmodes is studied in a two-dimensional kinetic analysis and will be reported in a separate paper. The onset of the instability gives rise to a new mechanism of the energy and momentum transfer between various plasma species and also affects the plasma transport process. These are open for further analysis.

Acknowledgments

The authors wish to thank Drs. T. Tsunematsu and S. Tokuda of Japan Atomic Energy Research Institute (JAERI) for useful comments and help in developing the numerical method. Thanks are also due to Dr. Y. Obata of JAERI, Prof. K. Nisikawa of Hiroshima University and Prof. Y. Furutani of Okayama University for continuous encouragements. The discussion with Dr. S. M. Mahajan, Prof. D. W. Ross of Univ. of Texas at Austin is elucidating. Two of the authors (K. I. and S. I. I.) are grateful to Prof. M. N. Rosenbluth for discussions and kind hospitalities during their stay at IFS under the U.S./JAPAN Joint Institute for Fusion Theory, (JIFT) where this work is completed.

References

1. See, for instance, papers in Heating in Toroidal Plasmas (C. Gormezano, G. G. Leotta and E. Sindoni, ed.; Commission of the European Communities, 1982) Vol. 1.
2. K. Itoh and S. Inoue, Comments Plasma Phys. Cont. Fusion 5(1980) 203.
3. K. Ikuta and T. Hatori, Japanese J. Appl. Phys. 20(1981) L595.
4. T. Hatori, T. Watanabe, H. Obayashi, T. Sato, S. Hiroe, T. Watari, T. Shoji, K. Adati, J. Jacquinot and A. Miyahara, Plasma Physics and Controlled Nuclear Fusion Research (IAEA, Vienna, 1975) Vol. 2, p.663.
5. T. H. Stix, The Theory of Plasma Waves (McGraw-Hill, New York, 1962) and Nucl. Fusion 15(1975) 737.
6. B. D. McVay, Nuc. Fusion 19(1979) 461.
7. Y. Lapierre, 2nd Joint Grenoble-Varenna Int. Symp. on Heating in Toroidal Plasma (Como, 1980) Vol. 1, p. 549.
8. S.-I. Itoh, K. Itoh and A. Fukuyama, Research Report IFSR #74 (University of Texas at Austin, 1982).
9. A. Fukuyama, S. Nishiyama, K. Itoh and S.-I. Itoh, Research Report HIFT-68 (Hiroshima Univ., 1982).
10. C. F. F. Karney, F. W. Perkins and Y.-C. Sun, Phys. Rev. Lett. 42(1979) 1621.
11. Equipe TFR, p. 225 in Ref. [1].
12. M. Ichimura, A. Aoki, J. Fujita, S. Hidekuma, S. Hirokura, et.al., Proc. Int. Conf. on Plasma Physics (Göteborg, 1982) Vol. 1, 125.

13. K. Appert, B. Bale, R. Gruber, F. Troyon, T. Tsunematsu and J. Voclavik, Nucl. Fusion 22(1982) 903.

14. S.-I. Itoh, K. Itoh and A. Fukuyama, "2-D Kinetic Analysis of ICRF waves in Tokamaks", paper presented at Fifth Topical Conf. on Radio Frequency Plasma Heating (Madison, 1983).

Appendix - Numerical Method

We briefly describe the numerical method to solve Eqs. (7) and (8) with the boundary conditions (9)-(11).

The grid points are constructed by introducing the radial and poloidal meshes. The grid points are defined in the upper-half plane ($0 < \theta < \pi$, $0 < r \leq a$) and the field is given in the sum of the even part and odd part such as

$$f(r,\theta) = f^e(r,\theta) + f^o(r,\theta) \tag{A1}$$

where $f^e(r,-\theta) = f^e(r,\theta)$ and $f^o(r,-\theta) = -f^o(r,\theta)$ are satisfied. In the dimensionless form

$$f \equiv uE_r \ , \ g \equiv uE_\theta \quad \text{and} \quad u \equiv r/a \tag{A2}$$

we have

$$u \frac{\partial^2 g^o}{\partial\theta\partial u} - \frac{\partial^2 f^e}{\partial\theta^2} + M_{11} f^e + M_{12} g^e = 0 \tag{A3}$$

$$u \frac{\partial^2 g^e}{\partial\theta\partial u} - \frac{\partial^2 f^o}{\partial\theta^2} + M_{11} f^o + M_{12} g^o = 0 \tag{A4}$$

$$-u^2 \frac{\partial^2 g^e}{\partial u^2} + u \frac{\partial g^e}{\partial u} - 2 \frac{\partial f^o}{\partial\theta} + u \frac{\partial^2 f^o}{\partial\theta\partial u} + M_{21} f^e + M_{22} g^e = 0 \tag{A5}$$

$$-u^2 \frac{\partial^2 g^o}{\partial u^2} + u \frac{\partial g^o}{\partial u} - 2 \frac{\partial f^e}{\partial\theta} + u \frac{\partial^2 f^e}{\partial\theta} + M_{21} f^o + M_{22} g^o = 0 \tag{A6}$$

where

$$M_{11} = M_{22} = u^2\left(k_\parallel^2 a^2 - \frac{a^2\omega^2}{c^2} S\right) \tag{A7-1}$$

$$M_{12} = -M_{21} = i\,\frac{u^2 a^2 \omega^2}{c^2} D \tag{A7-2}$$

The parity condition gives

$$\frac{\partial f^e}{\partial \Theta} = \frac{\partial g^e}{\partial \Theta} = f^o = g^o = 0 \quad \text{at} \quad \Theta = 0, \pi \tag{A8-1}$$

and the boundary condition gives

$$f^e = f^o = f^e = g^o = o \quad \text{at} \quad u = o\ . \tag{A8-2}$$

To take the advantage of this boundary conditions, we choose the poloidal mesh as

$$\Theta_m = \left(m - \frac{1}{2}\right)\Delta\Theta\ ,\ (m=1,\ldots,N_\Theta) \tag{A9-1}$$

$\Delta\Theta \equiv \pi/N_\Theta$, and the radial mesh

$$u_n = n \cdot h \qquad (n=1,\ldots,N_r) \tag{A9-2}$$

where $h \equiv 1/N_r$. On each (m,n) grid point, the field quantities such as $f^e_{m,n} \equiv f^e(u_n,\Theta_m)$ are defined. We introduce the vector $\vec{Y}_n$ defined by

$$\vec{Y}_n \equiv \begin{pmatrix} f^e_{1,n} \\ f^0_{1,n} \\ g^e_{1,n} \\ g^0_{1,n} \\ \vdots \\ f^e_{m,n} \\ \vdots \\ g^0_{L_\Theta,n} \end{pmatrix} \qquad (1 \leq n \leq N_r) \qquad \text{(A10)}$$

Then by approximating the differential operators by finite difference, the differential equations (A3)-(A6) are approximated by the linear set of equations such as

$$\vec{\vec{A}}_n \vec{Y}_{n-1} + \vec{\vec{B}}_n \vec{Y}_n + \vec{\vec{C}}_n \vec{Y}_{n+1} = 0 \quad (2 \leq n \leq N_r-1) \qquad \text{(A11-1)}$$

and

$$\vec{\vec{B}}_1 \vec{Y}_1 + \vec{\vec{C}}_1 \vec{Y}_2 = 0 \qquad \text{(A11-2)}$$

in the plasma. The coefficients $\vec{\vec{A}}_n$, $\vec{\vec{B}}_n$ and $\vec{\vec{C}}_n$ are the $4N_\Theta \times 4N_\Theta$ matrices and the partial differentials with respect to Θ appear in the off-diagonal elements of these matrices. The couplings between $\vec{Y}_{n-1}$, $\vec{Y}_n$ and $\vec{Y}_{n+1}$ are due to the radial differential operator, denoting the radial propagation of waves.

The solution in the vacuum region is given as

$$\begin{pmatrix} f \\ g \end{pmatrix} = \begin{pmatrix} f \\ g \end{pmatrix}_s + \begin{pmatrix} f \\ g \end{pmatrix}_g \tag{A12}$$

where the suffix s and g stand for the special solution and general solution respectively. When we take the cosine antenna such as $J(\Theta) = J_h \cos M\Theta$, we have

$$\begin{pmatrix} f \\ g \end{pmatrix}_s = \begin{cases} \begin{cases} \dfrac{Mc^2}{a^2\omega^2} \dfrac{J'_M(Kd/a)N_M(Ku)-J_M(Ku)N'_M(Kd/a)}{\{J'_M(Kd/a)N_M(Kd/a)-J_M(Kd/a)N'_M(Kd/a)\}} \sin(M\Theta) \\ \dfrac{u}{K} \dfrac{J'_M(Kd/a)N'_M(Ku)-J'_M(Ku)N'_M(Kd/a)}{\{J'_M(Kd/a)N''_M(Kd/a)-J''_M(Kd/a)N'_M(Kd/a)\}} \cos(M\Theta) \end{cases} \\ \times (-i\omega\mu_0 a J_h) \qquad 1 \leqslant u \leqslant d/a \\ 0 \qquad\qquad\qquad\qquad d/a \leqslant u \leqslant b/a \ , \end{cases} \tag{A13}$$

where J_M and N_M are the M-th order Bessel functions and $K \equiv \sqrt{\omega^2/c^2-k_\parallel^2}$ is the wave number in the vacuum. (If $k_\parallel^2 \geqslant \omega^2/c^2$ holds, K is redefined by $\sqrt{|\omega^2/c^2-k_\parallel^2|}$ and J_M and N_M are replaced by the modified Bessel functions I_M and K_M respectively.) The general solution is represented by the infinite Fourier sum. Since the number of the poloidal mesh point is N_Θ, the sum is truncated and we have

$$\begin{pmatrix} f \\ g \end{pmatrix}_g = \sum_{m=0}^{N_\Theta-1} \begin{matrix} -\frac{m}{K}\frac{[J_m'(Kb/a)N_m(Ku)-J_m(Ku)N_m'(Kb/a)]}{[J_m'(K)N_m'(Kb/a)-J_m'(Kb/a)N_m'(K)]}(\alpha_m \sin m\Theta - \beta_m \cos m\Theta) \\ -u\frac{[J_m'(Kb/a)N_m'(Ku)-J_m'(Ku)N_m'(Kb/a)]}{[J_m'(K)N_m'(Kb/a)-J_m'(Kb/a)N_m'(K)]}(\alpha_m \cos m\Theta + \beta_m \sin m\Theta) \end{matrix} \qquad \text{(A14)}$$

The unknown parameters $(a_0,\beta_0,\ldots,\alpha_{N_\Theta-1}, \beta_{N_\Theta-1})$ is determined by the boundary condition at u=1. By requiring that (f,g) and $(\partial f/\partial u, \partial g/\partial u)$ are continuous on the plasma surface and solving Eq. (11), we can determine all unknowns

$$\vec{Y}_1, \vec{Y}_2, \ldots, \vec{Y}_{N_r} \quad \text{and} \quad (\alpha_0,\ldots,\beta_{N_\Theta-1}) \ . \qquad \text{(A15)}$$

The total absorption is calculated by integrating the Poynting vector $\vec{S} = \frac{1}{\mu_0}\vec{E} \times \vec{B}$ over the plasma surface. We have (per unit length)

$$P_{in} \equiv -\int_0^{2\pi} a\, d\Theta\ S_r = \frac{\varepsilon_M}{2\omega\{_0 a^2}\frac{\pi}{2}\,\mathrm{Im}(\alpha_M^*)\{MC_r + C_\Theta(Ma_M+b_M) - C_{\Theta D}\} \qquad \text{(A16)}$$

where $\varepsilon_M = 2$ (M=0) or $1(M\neq 0)$,

$$a_m = \frac{m}{K}\frac{J_m'(Kb/a)N_m(K)-J_m(K)N_m'(Kb/a)}{J_m'(K)N_m'(Kb/a)-J_m'(Kb/a)N_m'(K)}\ , \qquad \text{(A17-1)}$$

$$b_m = K\frac{J_m''(K)N_m'(Kb/a)-J_m'(Kb/a)N_m''(K)}{J_m'(K)N_m'(Kb/a)-J_m'(Kb/a)N_m'(K)}\ , \qquad \text{(A17-2)}$$

$$C_r \equiv \frac{mc^2}{a^2\omega^2} \frac{J'_m(Kd/a)N_m(K)-J_m(K)N'_m(Kd/a)}{\{J'_m(Kd/a)N_m(Kd/a)-J_m(Kd/a)N'_m(Kd/a)\}}(-i\omega\mu_0 aJ_h), \quad \text{(A17-3)}$$

$$C_\Theta \equiv \frac{1}{K} \frac{J'_m(Kd/a)N'_m(K)-J'_m(K)N'_m(Kd/a)}{\{J'_m(Kd/a)N''_m(Kd/a)-J''_m(Kd/a)N'_m(Kd/a)\}} (-i\omega\mu_0 aJ_h) \quad \text{(A17-4)}$$

and

$$C_{\Theta D} \equiv -i\omega\mu_0 aJ_h \ . \quad \text{(A17-5)}$$

On the other hand, the absorbed power per unit length is calculated according to Eqs. (17) and (18) when the wave field $E_r(r,\Theta)$ and $E_\Theta(r,\Theta)$ is obtained. The numerical accuracy is examined by comparing P_{abs} and P_{in}. We find that the agreement between P_{abs} and P_{in} is good and the wave field show good convergence properties in changing N_Θ and N_r. More detailed arguments on the numerical procedure, accuracy and performance are presented in a separate paper.

Figure Captions

Figure 1 -

Contours of the radial-poloidal profile of the energy deposition $\dot{W}(r,\Theta)$ for the ion-ion hybrid resonance case where we take $\omega/\Omega_D(0) = 1.75$, $\nu/\omega = 10^{-2}$ and $k_\parallel a = 2$(a) and $k_\parallel a = 4$(b). Other parameters are standard; $a/R = 0.2$, $n_H/n_D = 0.1$, $\omega_{pD}^2(0)/\Omega_D^2(0) = 10^3$, $a^2\Omega_D^2(0)/c^2 = 5 \times 10^{-2}$ and $m_H/m_e = 1836$. The dotted line is the antenna at $d/a = 1.1$ and the shell is at $b/a = 1.5$. Also shown are the ion-ion hybrid resonance surface, the cut-off surface, and the cyclotron resonance surface of hydrogen. One sees that the energy deposition profile is localized both in x and y directions.

Figure 2 -

The ν/ω dependence of the maximum value of $\dot{W}(r,\Theta)$ and the absorption $P_{abs} = \int r dr d\Theta\, \dot{W}$ for the case of the ion-ion hybrid resonance ($|J_A| = 1$). P_{abs} (solid line) and $\dot{W}_{max}$ (dashed line) are given in arbitrary units. $\omega/\Omega_D(0) = 1.75$ and $k_\parallel a = 1$. Other parameters are standard. The relations $\dot{W}_{max} \sim \nu^{-1}$ and $P_{abs} \sim \nu^0$ are approximately satisfied.

Figure 3 -

The $k_\parallel$ dependence of absorption power (in $\omega\mu_0 a^2 J^2$ unit) for the ion-ion hybrid resonance ($\omega/\Omega_D(0) = 1.75$, $\nu/\omega = 10^{-2}$). A broad profile is obtained. The dashed line shows the case of much peaked density profile which has much lower critical $k_\parallel$ value which is denoted by the arrow.

Figure 4 -

The contour of $P_{abs}(k_{\parallel},\omega)$ for the fixed antenna current and the standard values of parameters and $\nu/\omega = 10^{-2}$. Unit is measured in $0.1(\omega\mu_0 a^2 J^2)$. The broad peak in the parameter range $1.6 \lesssim \omega/\Omega_D(0) \lesssim 2.2$ is due to the ion-ion hybrid resonance. Sharp peaks of P_{abs} is obtained when the cavity resonance condition is satisfied.

Figure 5 -

Power deposition profile for the case of cavity resonance on the mid-plane ($x=r\cos\theta$). $\omega/\Omega_D(0) = 2.75$, $k_{\parallel}a = 0.1$, $\nu/\omega = 10^{-2}$. This is the 5-th cavity mode, which is characterized by the four node circles and one node point near the axis on the r-θ-plane. Energy deposition extends whole plasma column. $x \leftrightarrow -x$ symmetry is weakly broken due to the toroidality.

Figure 6 -

The ν/ω dependences of the maximum values of $|\tilde{E}(r,\theta)|$ and $\dot{W}(r,\theta)$ and the power absorption P_{abs} for the case of the cavity resonance ($|J_A| = 1$). P_{abs} (solid line), $\dot{W}_{max}$ (dashed line) and $|E|_{max}$ (dashed and dotted line) are given in arbitrary units. $\omega/\Omega_D(0) = 2.8$, and $k_{\parallel}a = 1$. Other parameters are standard. The relations P_{abs}, $\dot{W}_{max}$, $|E|_{max} \propto \nu^{-1}$ are shown.

Figure 7 -

The $k_{\parallel}$ dependence of absorption power P_{abs} (in $\omega\mu_0 a^2 J^2$ unit) for the cavity resonance ($\omega/\Omega_D(0) = 2.5$) for $\nu/\omega = 0.005$, 0.01 and 0.015. The Lorentz type resonance is found. The width of the peak is proportional to ν/ω while the peak height is inversely proportional to ν/ω.

Figure 8 -

The total power absorption and the loading resistance $\hat{R}$ (in $a\omega\mu_0$ unit) are shown as a function of $\omega/\Omega_D(0)$. ν/ω is chosen to be 10^{-2}. The data denoted by Δ is calculated by choosing $\nu/\omega = 5 \times 10^{-3}$, showing weak dependence of P_{tot} (or $\hat{R}$) on ν. Other parameters are standard. $\hat{R}$ is measured in Ohm, and a in m.

Figure 9 -

Power deposition profiles $\dot{W}$ for low-field-side excitation (a) and high-field-side excitation (b). $\omega/\Omega_D(0) = 2.0$, $\nu/\omega = 10^{-2}$ and $k_{\parallel}a = 1.5$(a) and 2.5(b). x_r and x_c denote the ion-ion hybrid resonance and cut-off surfaces respectively.

Figure 10 -

Δ-dependence of P_{abs} (in $\omega\mu_0 a^2 J^2$ unit) for the high-field-side excitation. Δ is proportional to the poloidal length of the antenna. $k_{\parallel} = 1.5$, $\nu/\omega = 10^{-2}$ and $\omega/\Omega_D(0) = 2.0$ (solid line) and 1.75 (dashed line).

Figure 11 -

ν/ω-dependence of P_{abs} (in $\omega/\mu_0 a^2 J^2$ unit) for the low-field-side excitation. Cases of $\Delta = 0.2$ and 0.5 are compared for the parameter of the hybrid resonance ($\omega/\Omega_D(0) = 1.75$, $k_\parallel a = 1.5$). When Δ is small P_{abs} goes to zero as ν/ω vanishes. (Δ is proportional to the poloidal length of the antenna.) Similar trend is shown for the case $\omega/\Omega_D(0) = 2.5$, $\Delta = .2$ (dashed and dotted line) where neither the ion-ion hybrid resonance condition nor the cavity resonance condition is satisfied. When Δ becomes large, finite size effect appears.

Figure 12 -

Poynting vectors on the grid points for low-field-side excitation. Parameters are $k_\parallel a = 1.5$, $\omega/\Omega_D(0) = 1.75$, $\omega_{pD}^2(0)/\Omega_D^2(0) = 10^2$, $a^2\Omega_D^2/c^2 = 0.25$ and $\nu/\omega = 10^{-1}$.

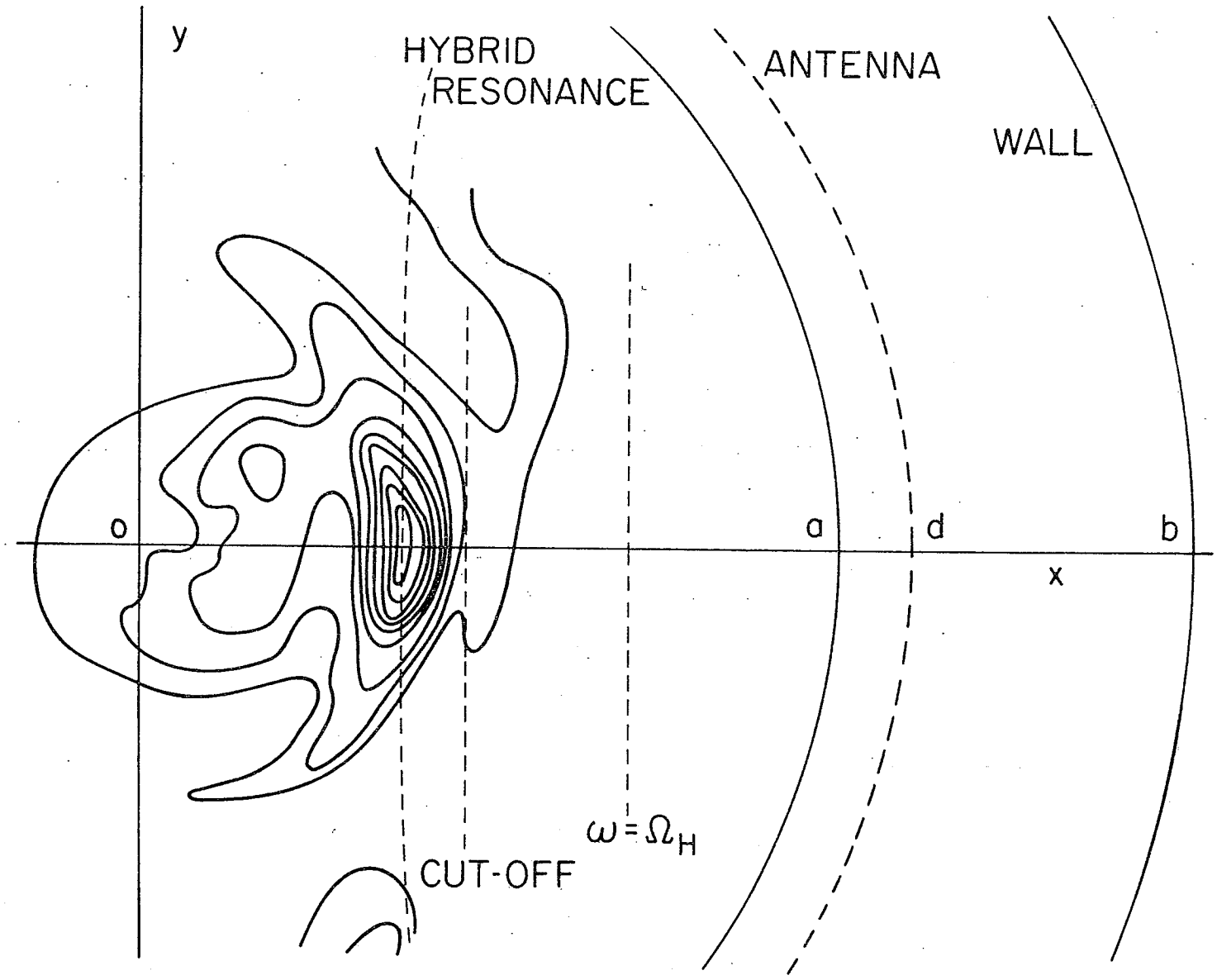

FIG. 1(a)

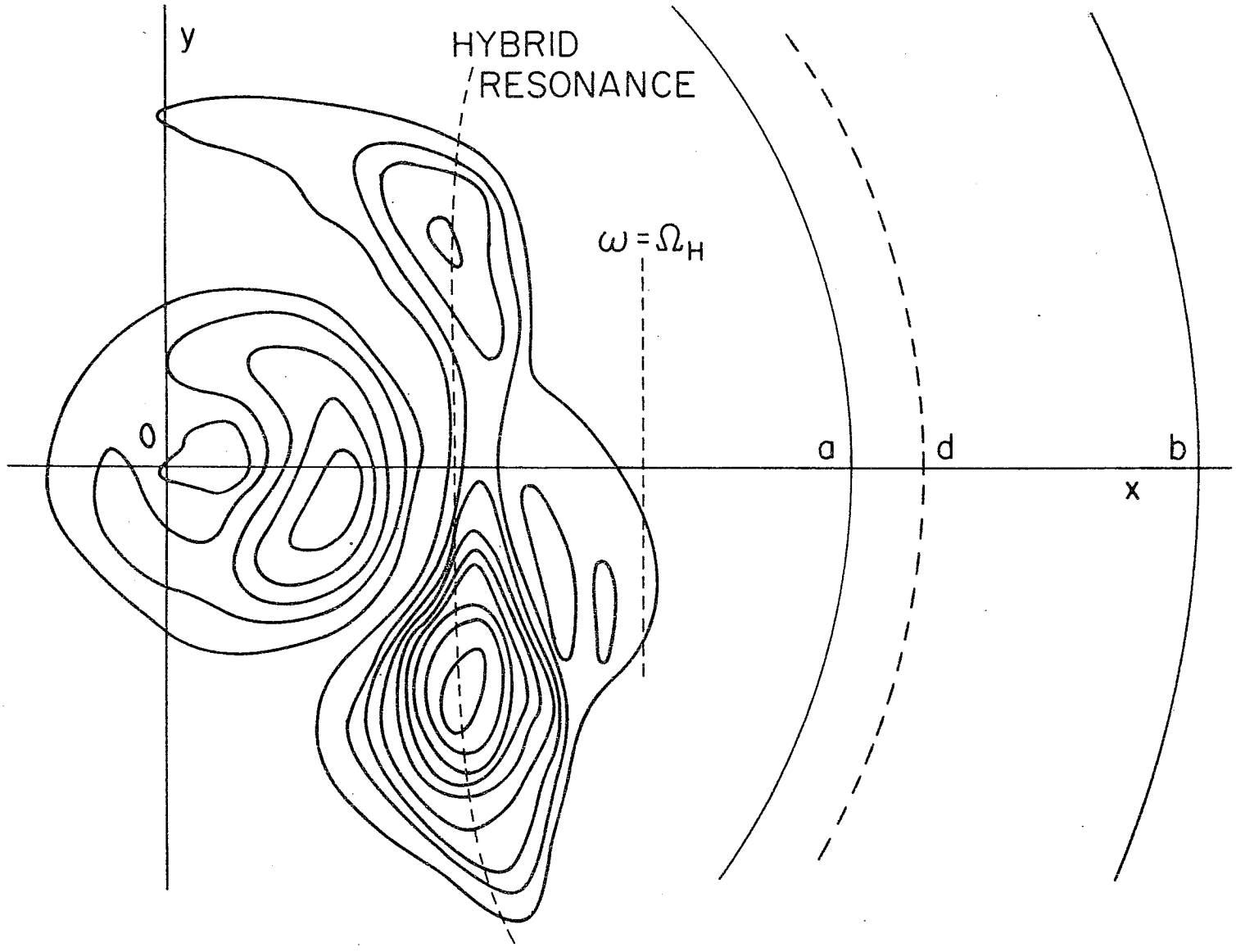

FIG. 1(b)

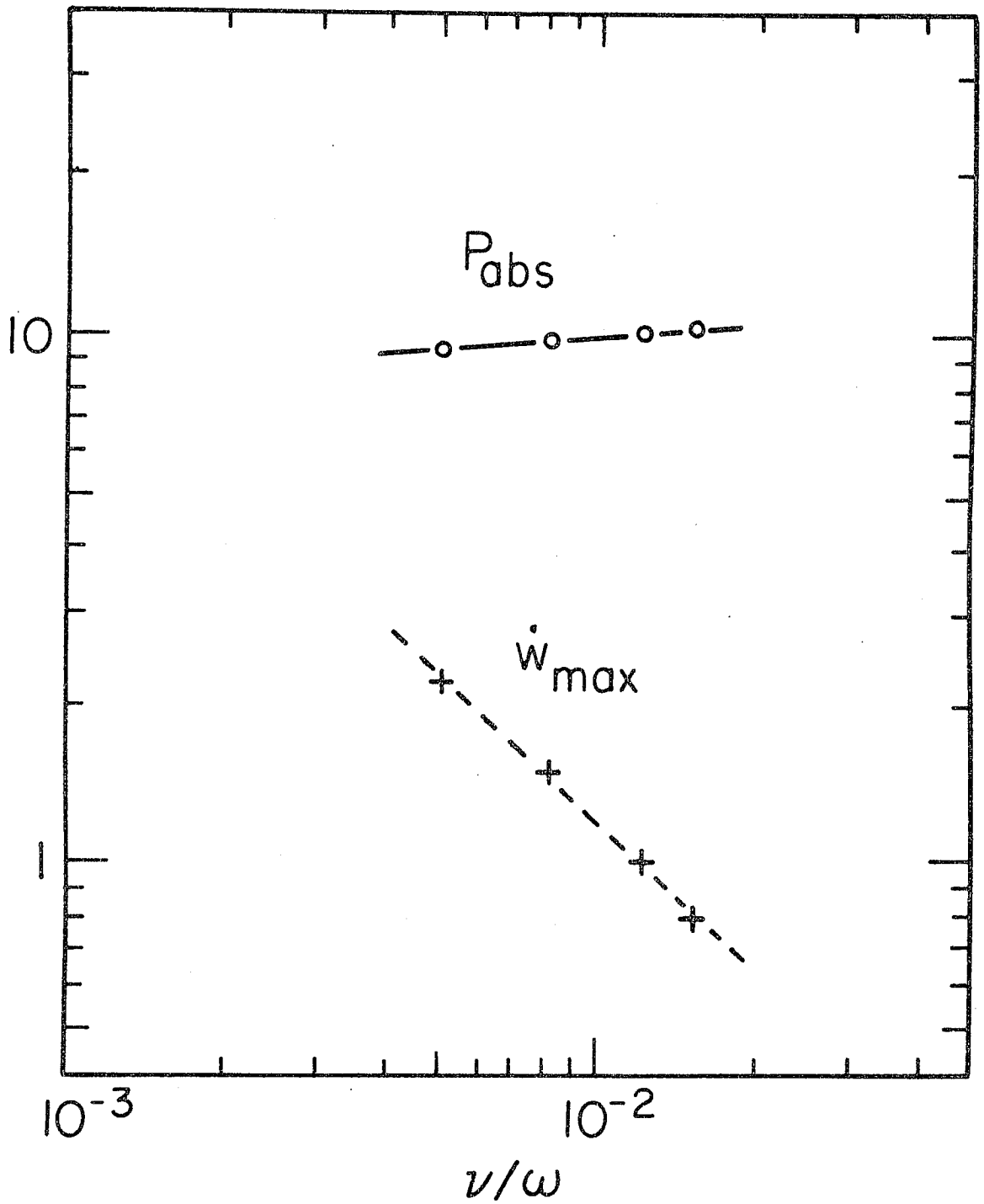

FIG. 2

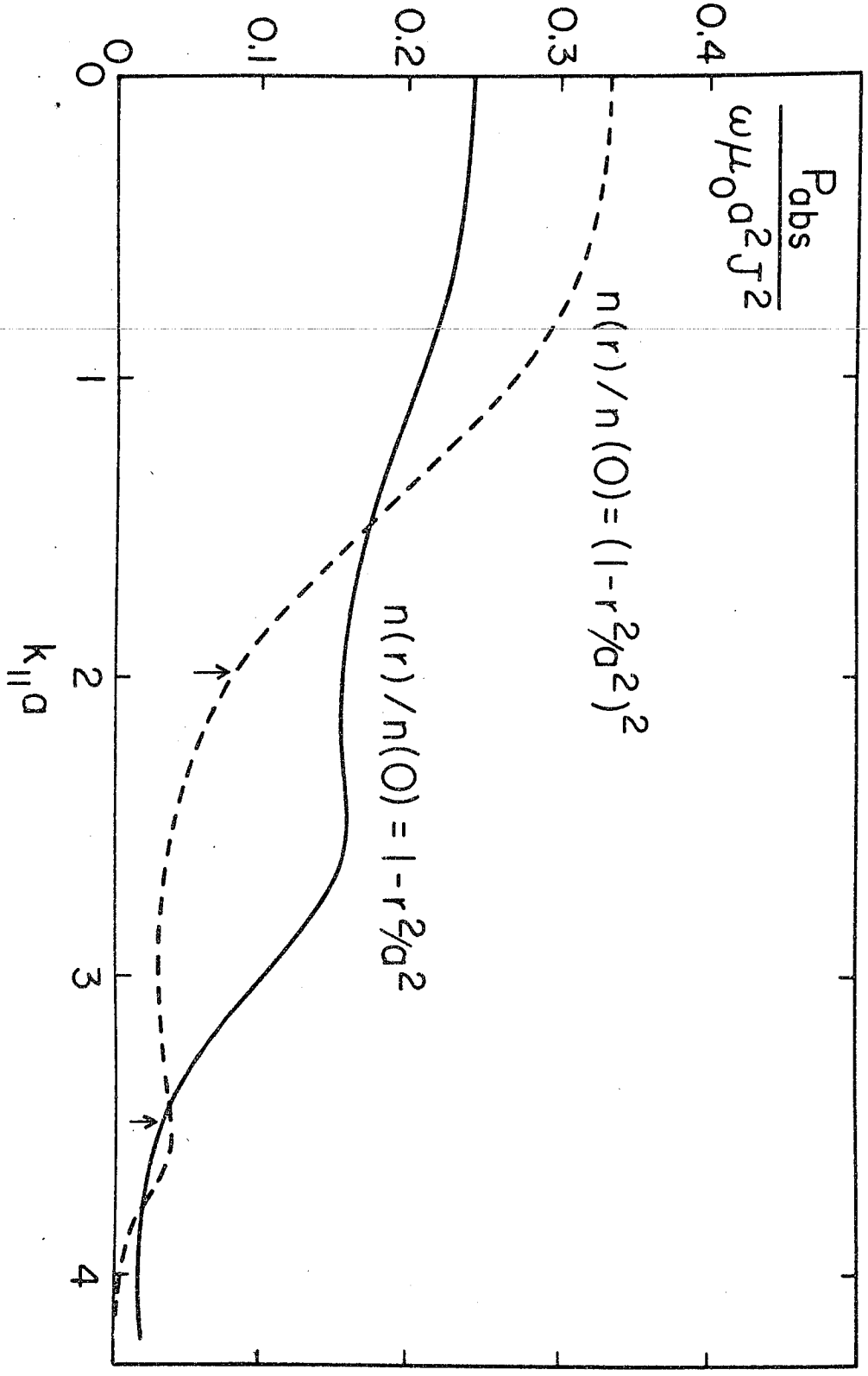
0
0.1
0.2
0.3
0.4
$\frac{P_{abs}}{\omega\mu_0 a^2 J^2}$
$n(r)/n(0) = (1 - r^2/a^2)^2$
$n(r)/n(0) = 1 - r^2/a^2$
0
1
2
3
4
$k_{\parallel} a$

FIG. 3

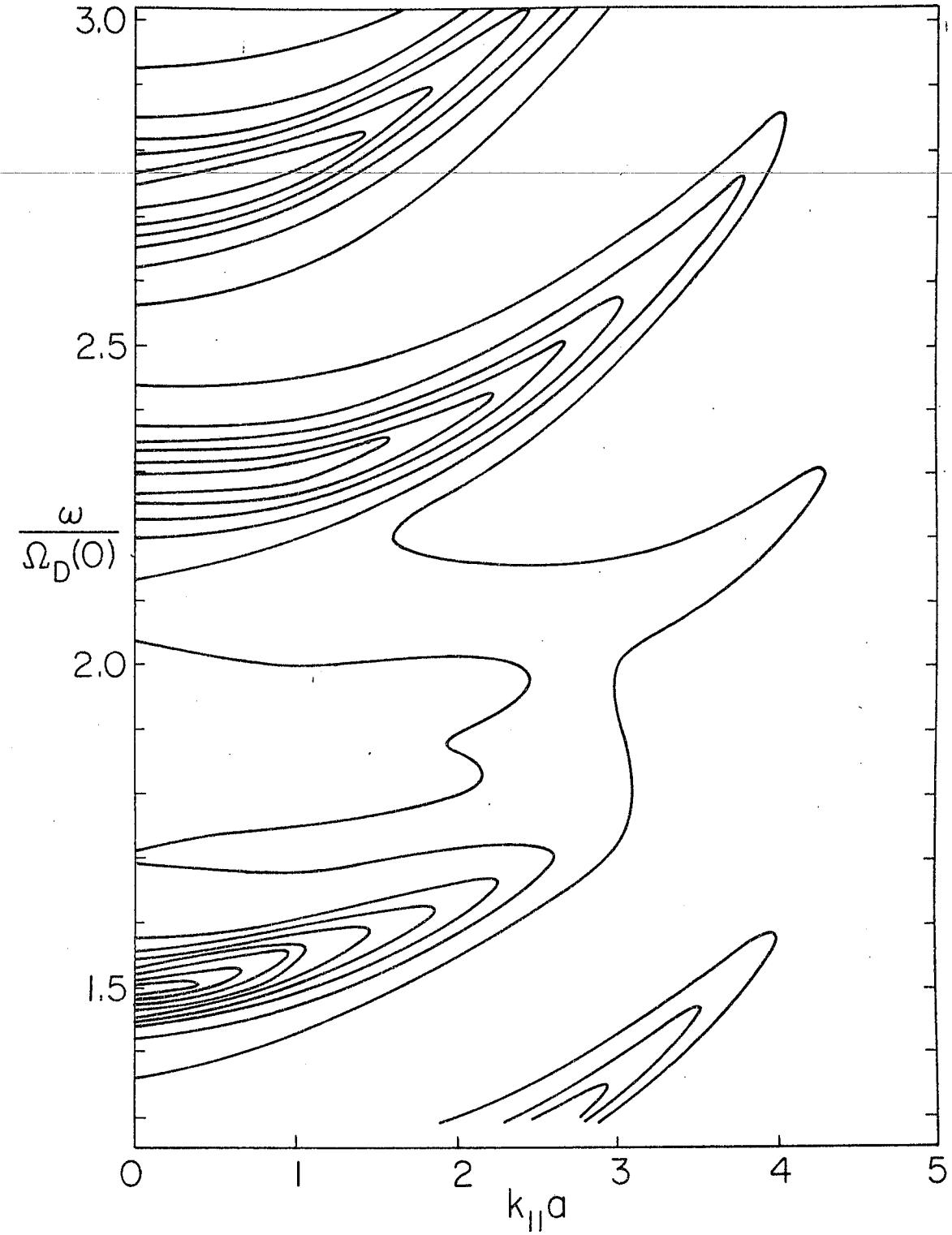

FIG. 4

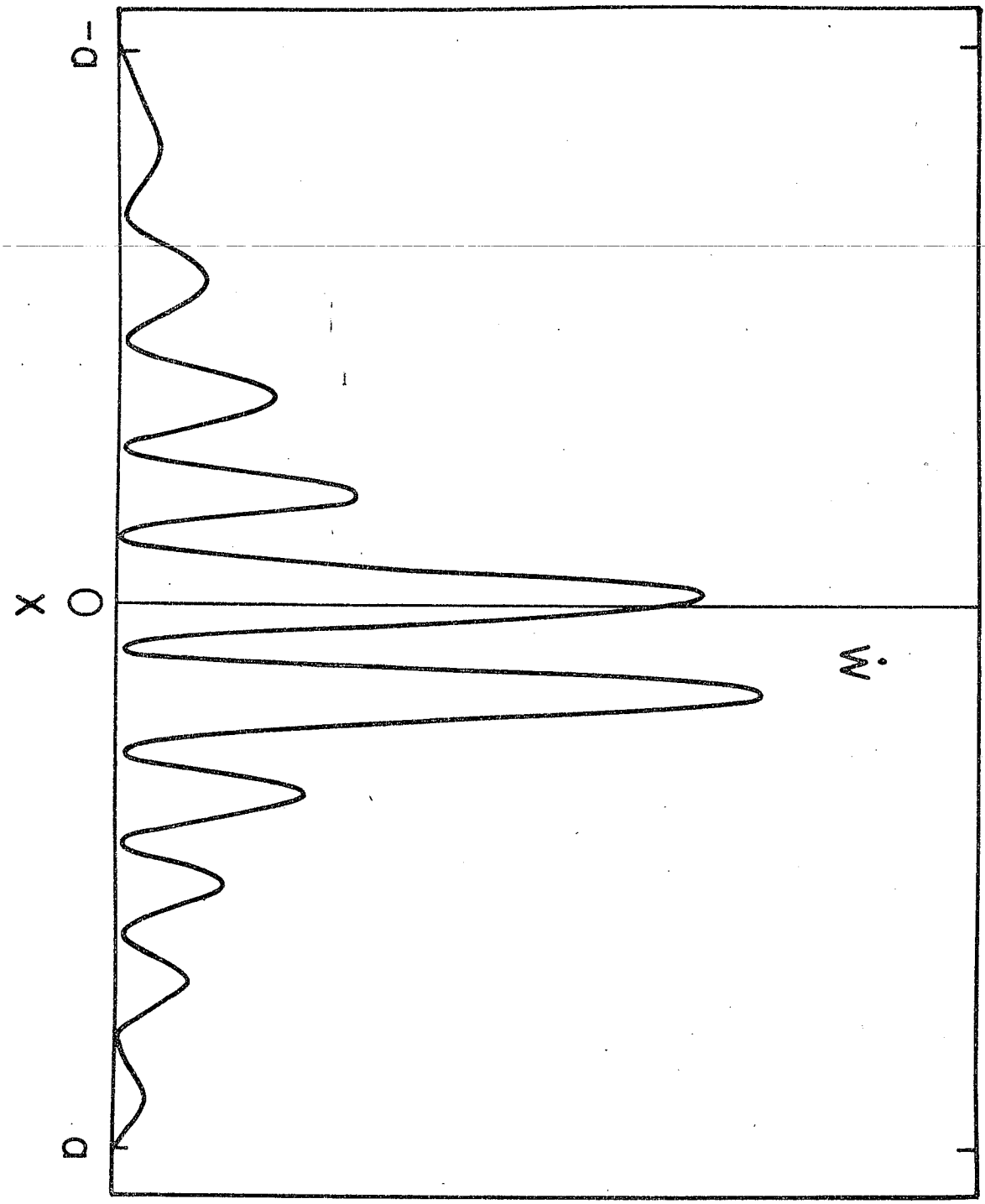

FIG. 5

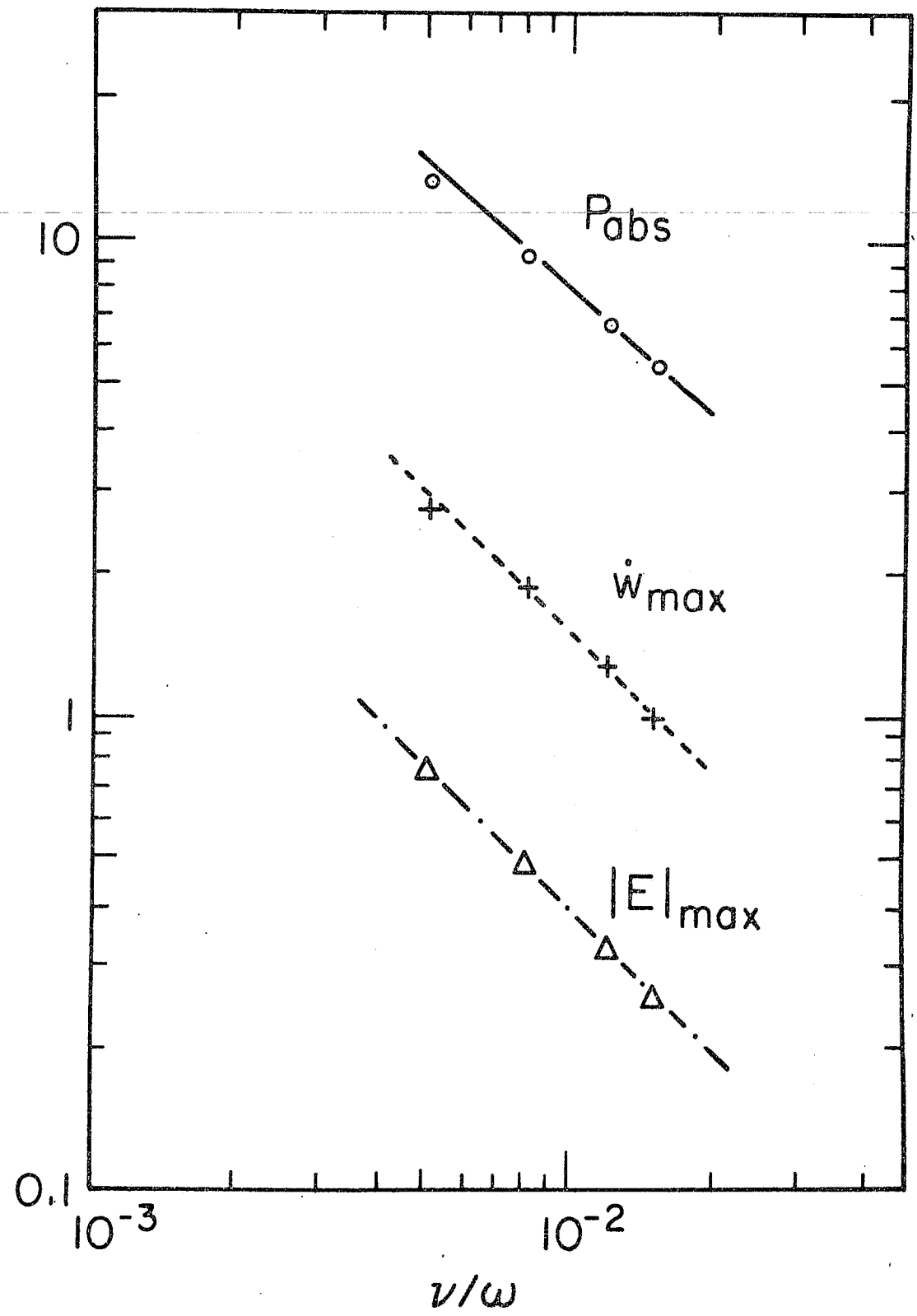

FIG. 6

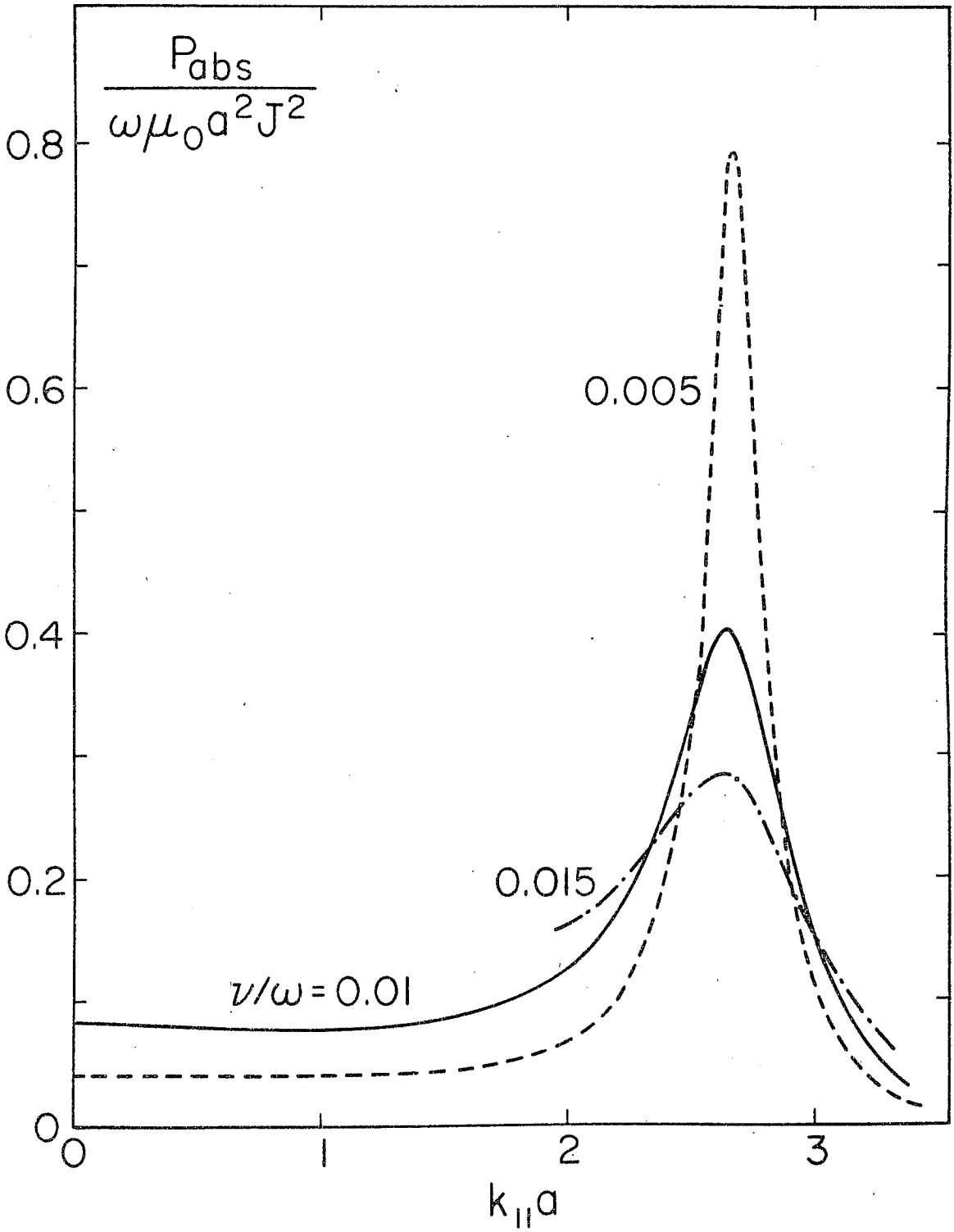
$\frac{P_{abs}}{\omega\mu_0 a^2 J^2}$
0.8
0.6
0.4
0.2
0
0
1
2
3
$k_{11}a$
0.005
0.015
$\nu/\omega = 0.01$

FIG. 7

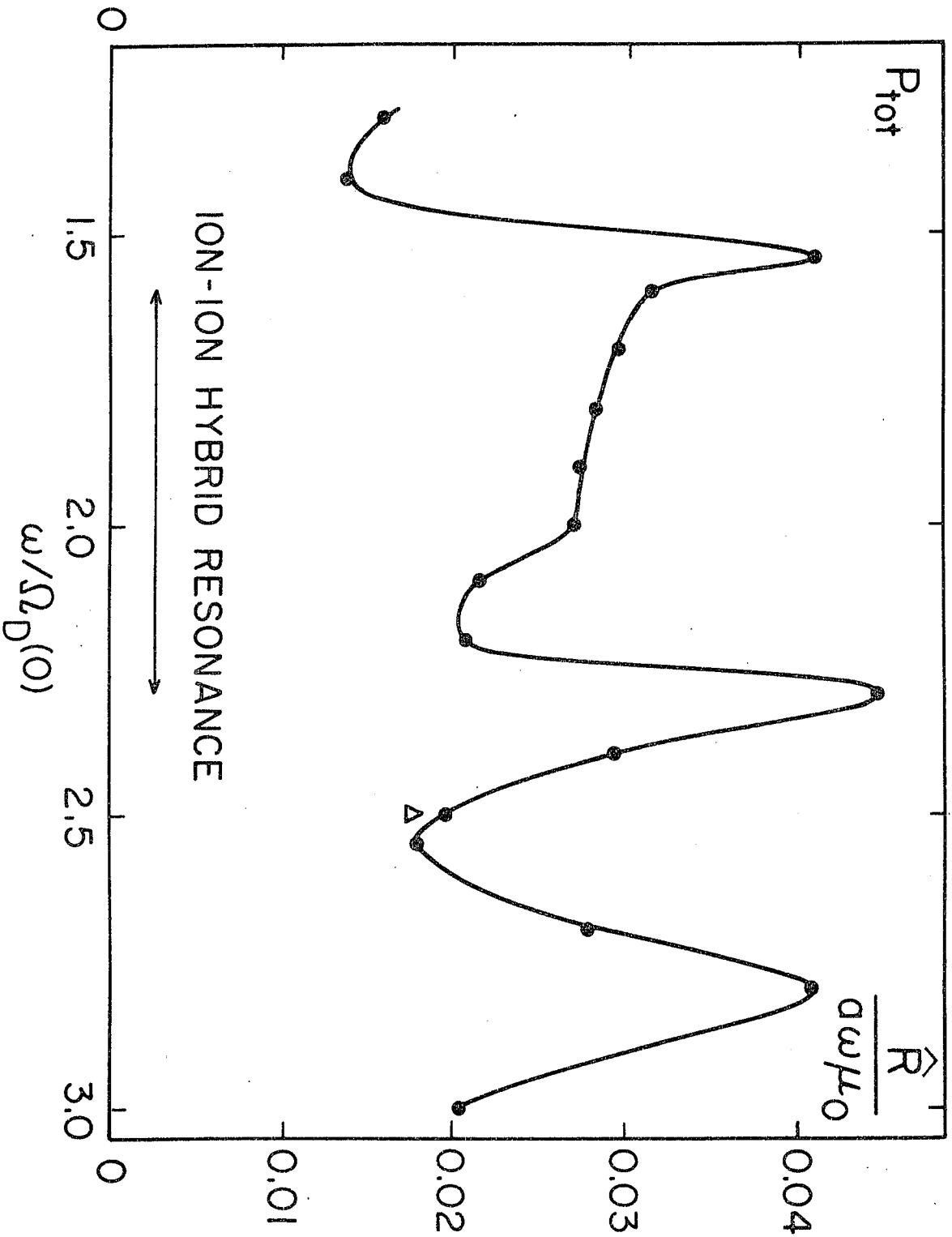
P_{tot}
$\frac{\hat{R}}{a\omega\mu_0}$
ION-ION HYBRID RESONANCE
$\omega/\Omega_D(0)$
0
1.5
2.0
2.5
3.0
0
0.01
0.02
0.03
0.04

FIG. 8

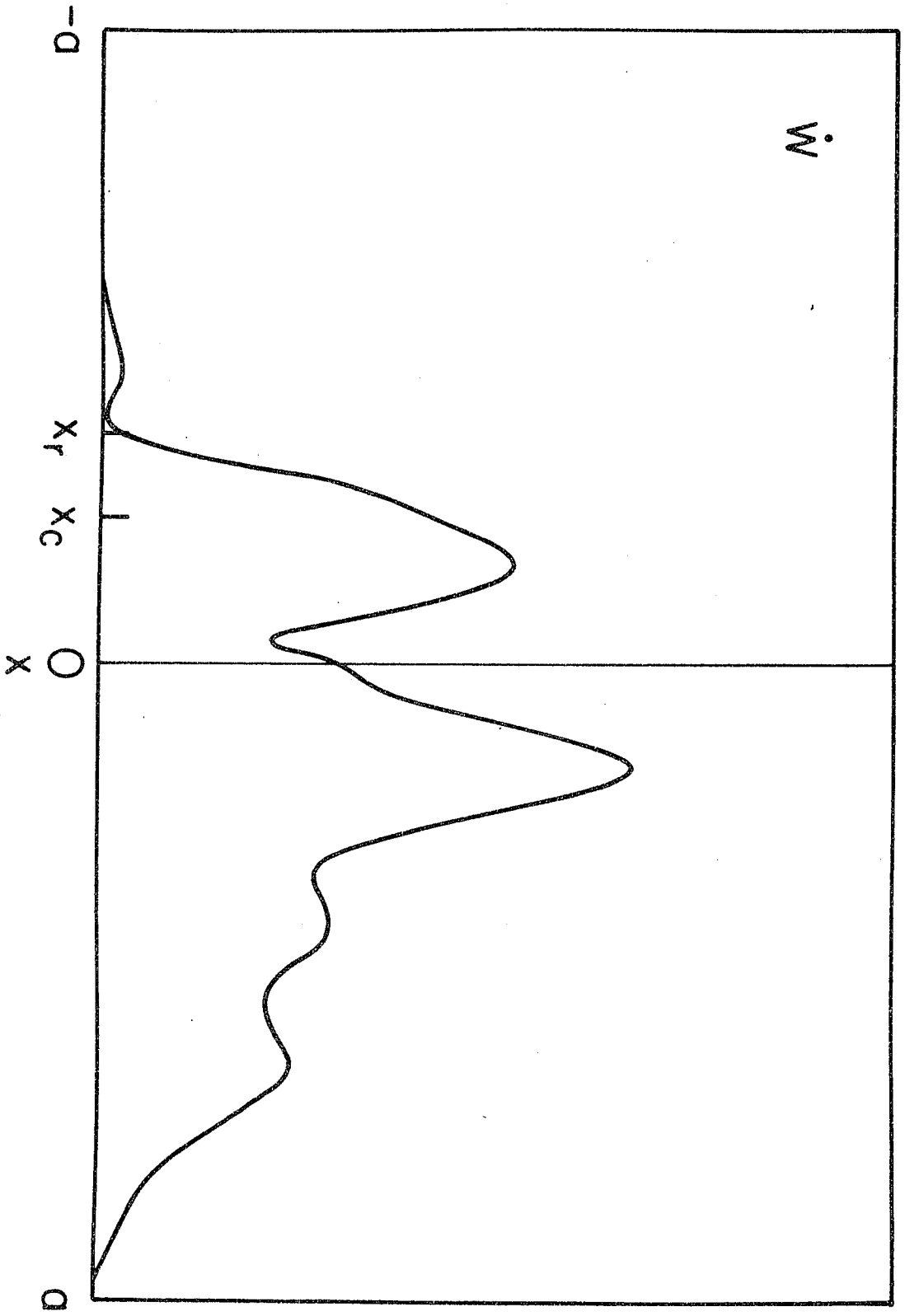

FIG. 9(a)

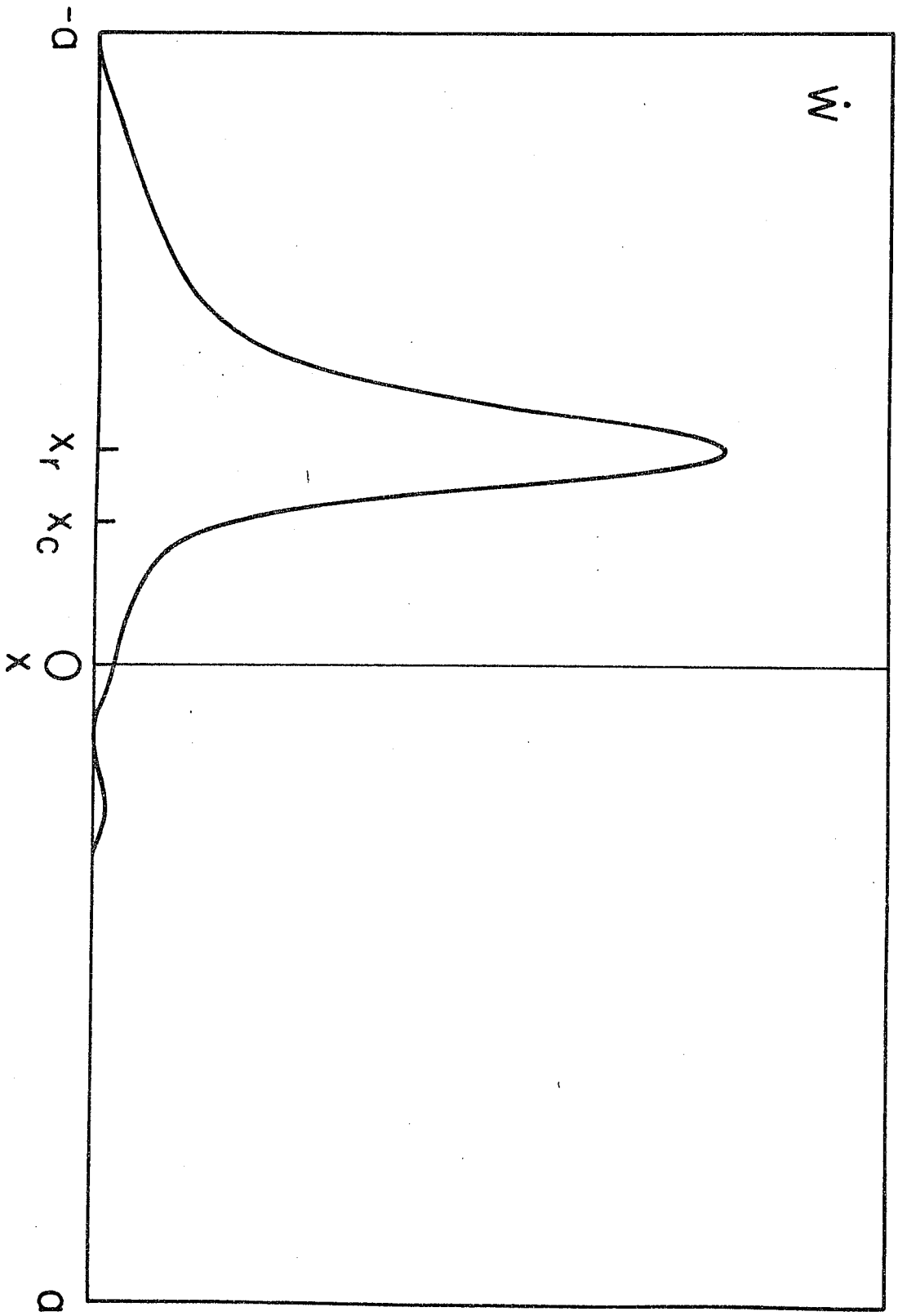

FIG. 9(b)

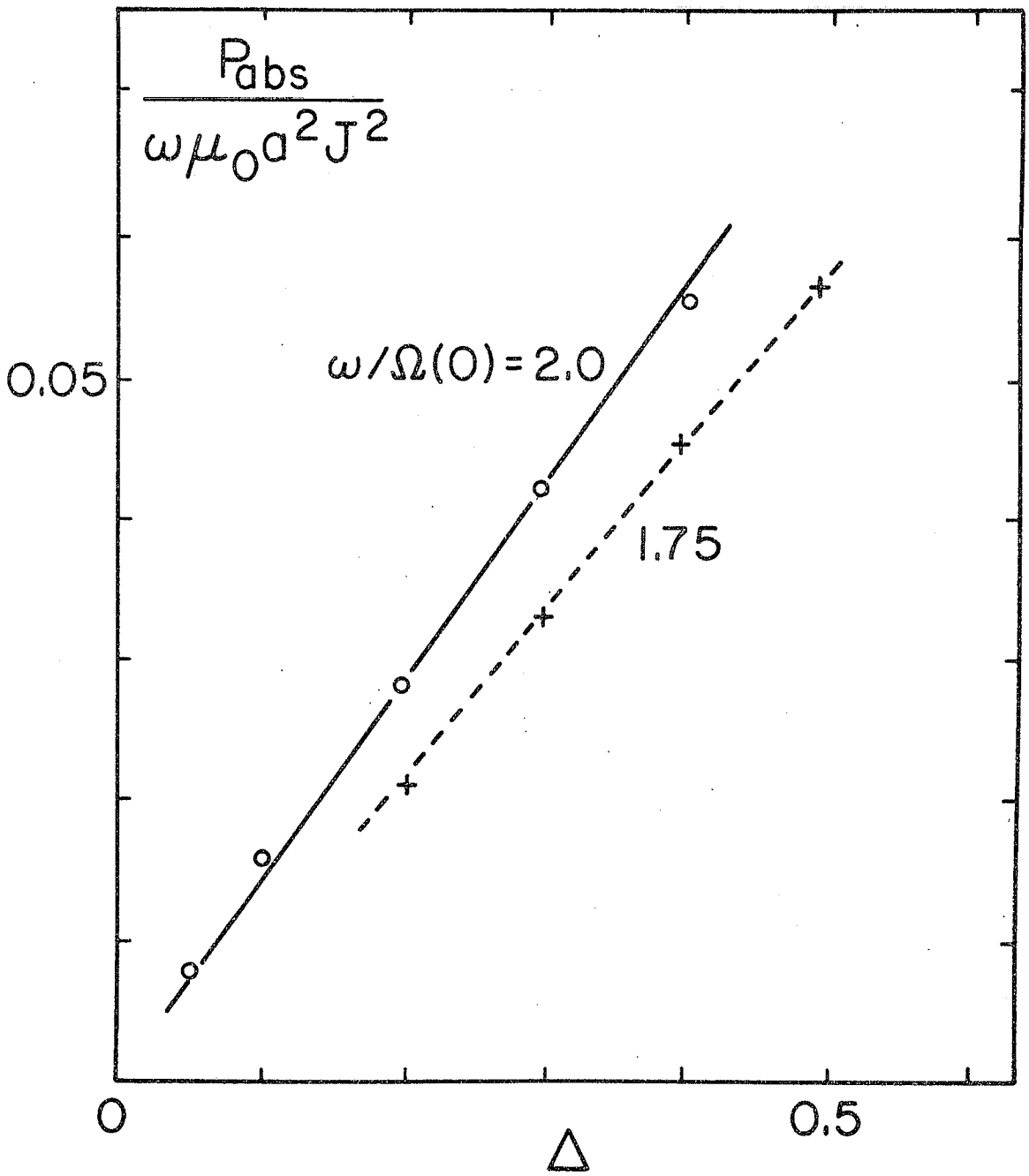

FIG. 10

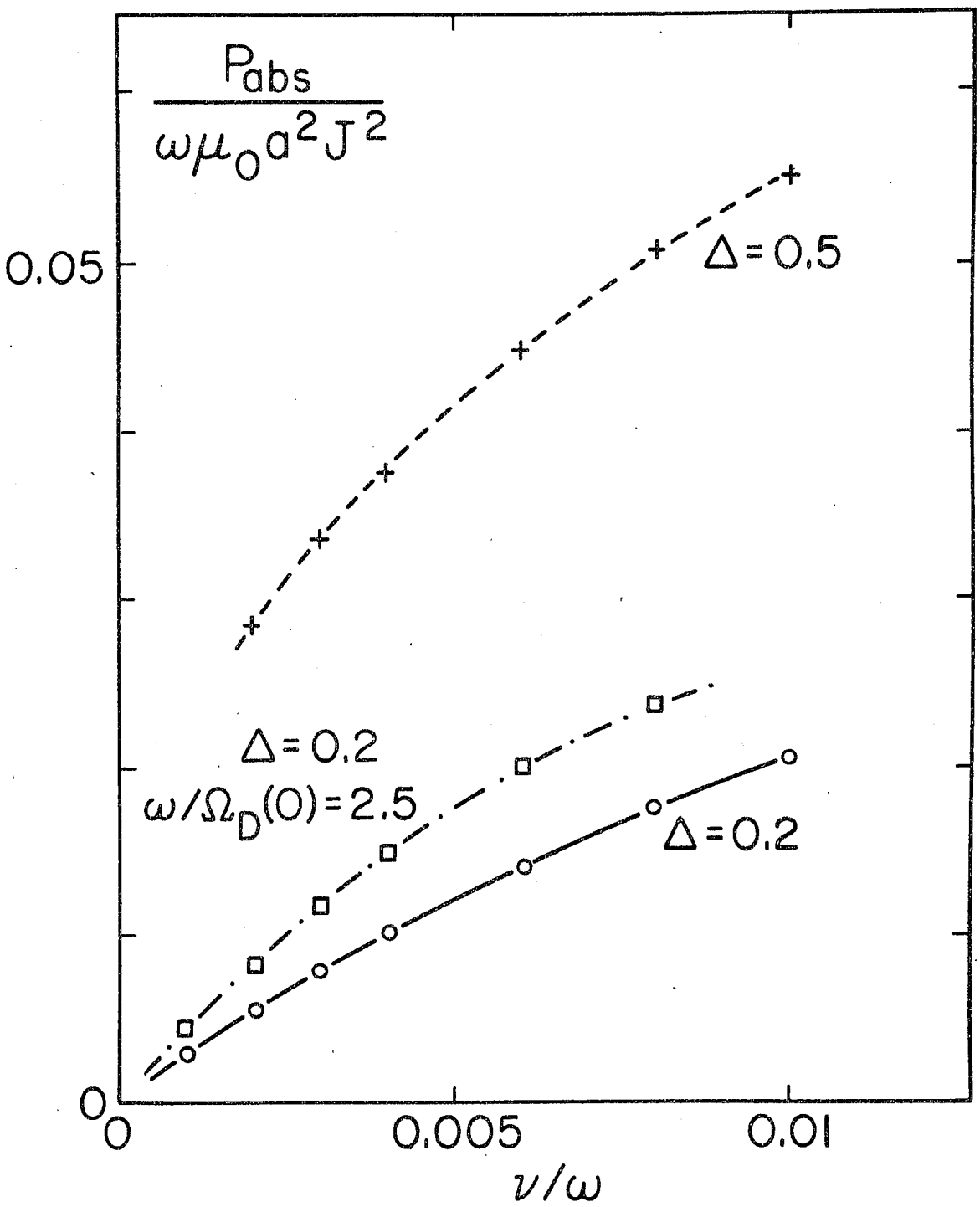
$\frac{P_{abs}}{\omega\mu_0 a^2 J^2}$
0.05
0
0
0.005
0.01
ν/ω
$\Delta = 0.5$
$\Delta = 0.2$
$\omega/\Omega_D(0) = 2.5$
$\Delta = 0.2$

FIG. 11

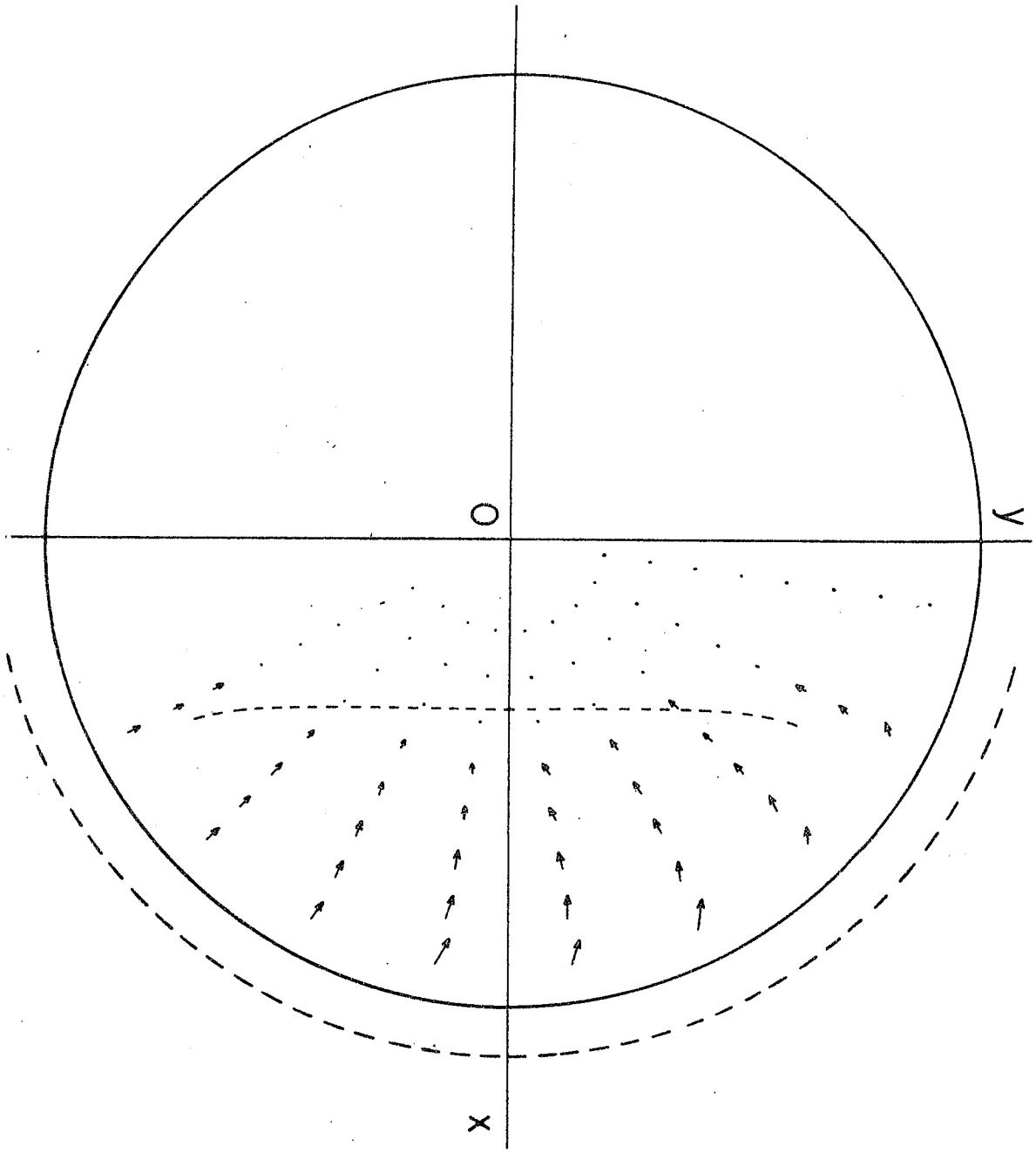

FIG. 12